ISSN 0022-4766, Journal of Structural Chemistry, 2021, Vol. 62, No. 3, pp. 331-355. © Pleiades Publishing, Ltd., 2021.
Russian Text © The Author(s), 2021, published in Zhurnal Strukturnoi Khimii, 2021, Vol. 62, No. 3, pp. 355-381.

HIGH-VALENCE CLUSTER COMPOUNDS OF TRANSITION METALS CONTAINING INTERSTITIAL HETEROATOMS: GEOMETRY, ELECTRONIC STRUCTURE, AND PHYSICOCHEMICAL PROPERTIES

Ya. M. Gayfulin[1], Yu. V. Mironov[1], and N. G. Naumov[1]*

The article reviews the current state of the chemistry of high-valence cluster compounds of group 3-7 transition metals containing interstitial heteroatoms. The synthesis methods, reactivity, main structural types, and electronic structure of resulting compounds are discussed.

DOI: 10.1134/S002247662103001X

Keywords: cluster, transition metal, crystal structure, electronic structure.

INTRODUCTION

The formation of compounds with metal–metal bonds, i.e. cluster compounds, is typical of most *d*- and *f*-block elements of periods 4, 5 in low oxidation states. Numerous cluster compounds with polymeric structures (the first characterized compounds of this type) constituted an extensive independent branch of inorganic chemistry. In this review, the term "cluster" is used in the sense that was first introduced into chemistry by F. A. Cotton: a complex containing three or more metal atoms held together entirely or at least partially by metal–metal bonds [1]. These last years have demonstrated a significant increase in the number of works dedicated to discrete high-valence clusters of zirconium, molybdenum, tungsten, and rhenium with different numbers of atoms in the metal core. The focus has shifted from the studies of fundamental aspects of cluster chemistry to their functional properties as well the properties of materials based on cluster compounds. The data on the structure and properties of such compounds were summarized in a number of outstanding comprehensive reviews written by the leading experts in this field [2-9]. Even though tremendous progress has been achieved in the chemistry of clusters, there are currently no general reviews devoted to the structure and physicochemical properties of cluster compounds with interstitial heteroatoms. Since much data have been obtained these last years as far as physicochemical properties of such compounds, we have tried to summarize the available information on their synthesis, structure, and properties in the present review. We considered the clusters of group 3-7 metals with "inorganic" inner ligands whose interstitial atoms (heteroatoms with respect to the "empty" metal cluster) are surrounded by a closo-polyhedron of metal atoms. The designations of the ligands used in this review are shown on the example of an octahedral cluster in Fig. 1.

We also found it appropriate to consider compounds where the neighboring metal clusters are connected by an μ_6-*Z* atom surrounded by a closo-polyhedron of metal atoms.

[1]Nikolaev Institute of Inorganic Chemistry, Siberian Branch, Russian Academy of Sciences, Novosibirsk, Russia; *naumov@niic.nsc.ru. Original article submitted August 27, 2020; revised October 20, 2020; accepted October 21, 2020.

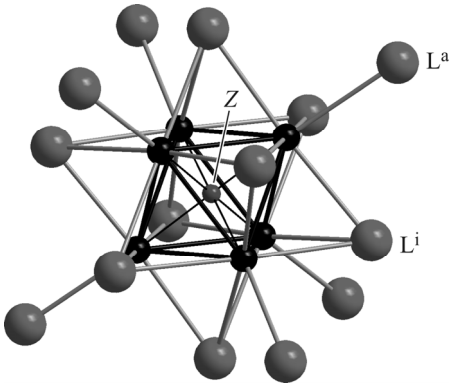

Fig. 1. Designations of the ligands on the example of an octahedral cluster: interstitial atom (heteroatom) (Z); "inner" μ_2 or μ_3 ligands coordinating the edges or the faces of the metal cluster (L^i); apical ligands (L^a).

High-temperature synthesis often yields polymer compounds whose neighboring cluster fragments are connected by bridging ligands. The structure of such compounds will be described using Schäfer's notation [10].

In general, the presence of bonding between metal atoms is a complicated question, especially in the cases of bridging atoms which often make critical contributions to the bonding energy of cluster cores [11]. This problem can be addressed by analysing the electronic structure of the studied compounds. In this review, we will consider compounds with such oxidation states of metal atoms and such metal–metal distances that ***permit*** the formation of metal–metal bonds; therefore, polynuclear complexes are excluded. Low-valence carbonyl clusters and cluster complexes with organic "inner" ligands were neither considered, since this is a vast independent branch of cluster chemistry.

METHODS FOR THE SYNTHESIS OF CLUSTERS WITH INTERSTITIAL ATOMS AND THEIR REACTIVITY

The methods for the synthesis of considered cluster compounds with interstitial atoms can be roughly classified into two main groups: high-temperature methods (conducted in closed systems, usually in sealed quartz evacuated ampoules or in metal containers) and solution methods. Chalcogenide and halide clusters with interstitial atoms are mainly prepared by high-temperature reactions, since the cluster core with an interstitial atom is formed only at high temperatures. The composition and structure of resulting compounds are largely determined by the reagent stoichiometry and by the synthesis temperature. After a cluster compound is prepared in the course of high-temperature synthesis, it can be further modified in solutions or in melts (zirconium, rhenium, and tungsten clusters with interstitial atoms). Differently are prepared clusters with interstitial (from one to seven) hydrogen atoms. Small size of hydrogen atoms and their ability to migrate inside the cluster core allow obtaining clusters with an interstitial atom also by self-assembly reactions at low temperatures in solutions and by reactions of hydrogen introduction into prepared clusters at moderate temperatures (400-500 °C).

Group 3. Rare-earth metal (REM) halide clusters are prepared in the course of long-term high-temperature (up to 1000 °C) reactions in sealed metal (niobium, tantalum) containers (e.g., see review paper [6]). The comproportionation of REM halides with a metal atom or controlled metallothermic reduction of REM halides by more active metals leads to the formation of clusters where the oxidation number of the metal is less than two and, therefore, there are electrons to form bonding within the metal cluster. The vast majority of such REM halides form polynuclear complexes, clusters $\{R_x\}$ containing atom *Z* or small groups of atoms in the polyhedron's center. The central atoms in polynuclear REM complexes may be non-metals (H, B, C, dimeric fragments C_2) as well as transition metals (Cr–Zn, Ru–Pd, and W–Au). Atom *Z* in such complexes is surrounded by metal atoms to form isolated clusters or polymeric chains, networks, and frameworks connected

by bridging ligands. The compositions and structures of these compounds will be discussed in the section "Types of structures and structural features of clusters with interstitial atoms". For actinides, the only known examples are octahedral thorium clusters. The reaction of Th and $ThBr_4$ in hydrogen or deuterium at 680 °C leads to the formation of black cubic crystals of compound $Th_6Br_{15}H_7$ and its deuterium analog [12]. The seven deuterium atoms are statistically distributed over the eight octahedron's faces. The authors of [13] reported the synthesis and structure of other thorium clusters: MTh_6Br_{15} (M = Mn, Fe, Co, Ni), $Na(x)FeTh_6Br_{15}$, and $Th_6Br_{14}C$. Their structure is similar to that of niobium halides Nb_6F_{15} and Nb_6Cl_{14}.

Group 4. For titanium, there is only one known cluster compound containing a complex with an introduced atom, namely, $[Ti_6CCl_{14}]$ [14]. This compound is formed by the reaction of $TiCl_3$ with metallic sodium in the atmosphere of Ar at 440-550 °C with paraffin used as the source of carbon.

A series of zirconium octahedral complexes with interstitial hydrogen atoms was obtained by the reaction of $ZrCl_4$ reduction using Bu_3SnH in a THF solution [15]. The consequent treatment by phosphines allowed isolating compounds $H_4Zr_6Cl_{14}(PR_3)_4$, (PR_3 = PMe_3, PEt_3) containing hydrogen atoms in their cluster cores, numerous anionic salts $[H_5Zr_6X_{18}]^{3-}$ (X = Cl, Br), and an unusual pentanuclear complex $[H_4Zr_5Cl_{12}(PMe_3)_5]$ [16-23]. These compounds were characterized structurally and by NMR.

Another method for the synthesis of octahedral zirconium complexes with interstitial atoms is based on the reaction of Zr, ZrX_4, Z and an alkali metal halide AX (if necessary) taken in a required stoichiometry. The reaction usually proceeds quantitatively to form phases with the composition $A_y\{Zr_6(Z)X^{i}_{12}\}X^{a}_{m}$ (where A is an alkali or alkaline earth metal (Li, Na, Ca, Ba)) [16-18, 20-25].

Many polymer compounds with the $\{Zr_6ZX_{12}\}$ core react with organic molecular and ionic compounds in solutions or melts in the course of depolymerization reactions. As a result of depolymerization, the bonds of Zr–X–Zr bridges are split and the ions or organic molecules are attached to Zr atoms to occupy vacant positions of terminal ligands. It was shown that depolymerization reactions are more probable for lower degrees of polymerization in the initial compound. There are two types of solvents that are used to make solutions of compounds with the $\{Zr_6ZX_{12}\}$ core. The first type are polar solvents such as CH_3CN [26-29], MeOH [30], and H_2O [31-34]. A necessary condition for the reaction is that the solution should contain an excess of a Lewis base (e.g., anions Cl^-) replacing vacant terminal positions in the metal cluster. In the course of the dissolution, the cluster core may undergo uncontrolled one- or two-electron oxidation to yield cluster complexes with less than 14 (or 18 in the case when Z is a transition metal) cluster skeletal electrons (CSEs). The first reported examples of such reactions were reactions of compounds $M_x[(Zr_6ZCl^{i}_{12})Cl^{a}_{n}]$ with Et_4NCl, Et_4PCl, $EtNH_2$, PEt_3, PMe_2Ph in CH_3CN. The second type of solvents for the preparation of solutions of $M_x[(Zr_6ZX_{12})X_n]$ compounds is low-temperature ionic liquids such as mixtures of 1-ethyl-3-methylimidazolium (ImCl) chloride with $AlCl_3$ that are used in the chemistry of zirconium clusters [35, 36]. A typical ImCl:$AlCl_3$ ratio for the required excess of chloride anions is 7:3-7:2. For example, the dissolution of cluster compounds $Rb_5[Zr_6BCl_{18}]$, $K[Zr_6CCl_{15}]$, $Li_2[Zr_6MnCl_{15}]$ in ionic liquid resulted in good yields of $(Im)_5[Zr_6BCl_{18}]C_6H_5CH_3{\cdot}2CH_3CN$, $(Im)_4[Zr_6BCl_{18}](Im)_4[Zr_6CCl_{18}]$, $(Im)_5[Zr_6MnCl_{18}]C_6H_5CH_3{\cdot}2CH_3CN$ [37, 38].

For hafnium, there are only a few known examples of compounds with the cluster core $[Hf_6ZCl_n]$ (Z = B, C) prepared by the high-temperature method. The authors of a study of ternary systems Hf–$HfCl_4$–Z synthesized and described cluster phases $[Hf_6ZCl_{14}]$, Z = B, C [39], $A[Hf_6ZCl_{14}]$ with A = Li, Na, K and Z = B, C with the Nb_6Cl_{14} type structure; $A[Hf_6ZCl_{15}]$ with A = K, Cs with the $CsK[Zr_6BCl_{15}]$ type structure; $Na_{0.8}[Hf_6BCl_{15}]$ with the Ta_6Cl_{15} type structure.

Group 5. Cluster complexes with an interstitial atom that are formed by group 5 metals are represented by a small number of compounds prepared mainly in the conditions of high-temperature synthesis. Cluster compound $K[V_3Te_3O_x]$ is prepared by the reaction between K_2Te_3, V, and Te taken in the 2:2:4 ratio at 900 °C in an evacuated quartz ampoule [40]. Heating the mixture of RbBr, Nb, $NbBr_5$, and S up to 800 °C yields complex $Rb_3[Nb_6SBr_{17}]$ with a 14-electron cluster anion $[Nb_6SBr_{18}]^{4-}$ [41]. Hydride derivatives HNb_6I_{11}, $CsHNb_6I_{11}$, and HNb_6SI_9 are formed upon heating phases Nb_6I_{11}, $CsNb_6I_{11}$, and Nb_6SI_9 in hydrogen at moderate temperatures (400-500 °C) [42-46].

Cluster complex $[V_6OSe_8(PMe_3)_6]$ with an octahedral metal core was obtained by the interaction of $[CpVCl_2(PMe_3)_2]$ with $Se(SiMe_3)_2$ in THF [47]. Compounds with the general formula $(ArN)_{14}Ta_6O$ (Ar = Ph, *p*-MeC_6H_4, *p*-$MeOC_6H_4$, *p*-*t*-BuC_6H_4, *p*-BrC_6H_4, *m*-ClC_6H_4) were obtained by the interaction of $Ta(NMe_2)_5$ or $(CH_2C_6H_5)_3Ta$ = N(*t*-Bu) with an excess of the corresponding aniline and with water [48].

Group 6. For molybdenum, there are two known compounds where the chalcogen atom is surrounded by six metal atoms: $Ba_4[Mo_{12}S_{18}]$ [49] and $Mo_6I_6Se_8$ [50]. These compounds were synthesized quantitatively by high-temperature reactions of stoichiometric amounts of initial substances.

For tungsten, a large family of cluster complexes with an interstitial atom (general formula $[W_6ZCl_{12}]$ (*Z* = C, N, O)) was obtained. The metal cluster of these complexes is trigonal-prismatic. Such complexes are formed using the reduction of higher tungsten chlorides by tungsten or other metals (Bi, Cu) in the presence of a carbon source or a nitrogen source. The authors of [51] synthesized and characterized cluster compounds with stoichiometries $[W_6CCl_{18}]$ and $[W_6CCl_{16}]$. The first one was obtained by a one week heating of W, WCl_6, and graphite in a quartz ampoule at a temperature gradient of 690/700 °C. The second one was prepared by heating W, WCl_5, and CCl_4 in a quartz ampoule at temperature gradient of 757/597 °C.

Reducing WCl_6 by metallic Bi in the presence of CCl_4 at 400 °C for 72 h yields black X-ray amorphous powder. Dissolving this powder in 1% HCl leads to the formation of anion $[W_6CCl_{18}]^{2-}$ isolated in the form of the $(Bu_4N)_2[W_6CCl_{18}]$ salt [52].

Another method for the preparation of $[W_6CCl_{18}]$ type compounds is the pyrolysis of the known octahedral cluster complex $[W_6Cl_{12}] = [(W_6Cl_8)Cl_2Cl_{4/2}]$ in the chlorinated hydrocarbon medium [53]. This method was used to obtain W_6CCl_{18}, W_6CCl_{16}, and a polymer compound $W_6CCl_{15} = [(W_6CCl^{i}_{11})Cl^{a}_{2}Cl^{a-a}_{4/2}]$ with cluster cores containing 11 inner chloride ligands instead of 12 ligands in previously known compounds of this type. The reduction of β-WCl_6 by metallic copper in the presence of hexachlorobenzene as a source of carbon yields copper salt $Cu[W_6CCl_{18}]$ [54]. The pyrolysis of W_6Cl_{12} in the C_6Br_6 medium yielded the compound whose octahedral cluster fragments $W_6X^{i}_{8}$ (*X* = Cl, Br) and trigonal prismatic fragments $W_6CX^{i}_{12}$ are combined in a polymeric structure $[(W_6CX^{i}_{12})X^{a}_{2}X^{a-a}_{4/2}]_2[(W_6X^{i}_{8})X^{a}_{3}X^{a-a}_{3/2}]_2[(W_6X^{i}_{8})X^{a-a}_{6/2}]$ with the empirical formula $W_{30}C_2(Cl,Br)_{68}$. The reduction of WCl_6 by metallic Bi in the presence of NaN_3 at 500 °C for 72 h yielded another trigonal prismatic tungsten cluster $Na[W_6NCl_{18}]$ containing a 24-electron cluster anion $[W_6NCl_{18}]^{-}$ with an interstitial nitrogen atom [55]. The compound is soluble in dilute hydrochloric acid to cause a spontaneous one-electron reduction of the cluster anion. The $[W_6NCl_{18}]^{2-}$ anion containing 25 CSEs was isolated in the form of compounds $(Bu_4N)_2[W_6NCl_{18}]$. Compounds $A[W_6ZCl_{18}]$ (*Z* = C, N; *A* = Li, Na, Cs, Ca, Ag) can also be obtained by the reduction of WCl_4 with cyanamides A_2CN_2 (ACN_2, *A* = Ca) [56, 57]. These compounds have a layered structure where the layers of cluster anions $[W_6ZCl_{18}]^{-/2-}$ alternate with the layers of cations A^{+} (A^{2+}, *A* = Ca). It was shown electrochemically that anion $[W_6CCl_{18}]^{2-}$ can exhibit both oxidation and reduction at moderate values of the potential. The oxidation of the anion in solution $(Bu_4N)_2[W_6CCl_{18}]$ in CH_3CN using $(NO)BF_4$ yielded anion $[W_6CCl_{18}]^{-}$ that was isolated in the form of compound $(Bu_4N)[W_6CCl_{18}]$.

Cyclic voltammetry confirmed that the cluster anion can be further reduced to the forms with oxidation numbers three and four. In this case, the $E_{1/2}$ value is –0.527 V for the pair $[W_6NCl_{18}]^{2-}/[W_6NCl_{18}]^{3-}$ and –1.800 V for the pair $[W_6NCl_{18}]^{2-}/[W_6NCl_{18}]^{3-}$ $[W_6NCl_{18}]^{3-}/[W_6NCl_{18}]^{4-}$. The chemical reduction of $[W_6NCl_{18}]^{2-}$ using Cp_2Co lead to the formation of anion $[W_6NCl_{18}]^{3-}$ that was isolated and studied in the form of compounds $(Bu_4N)_3[W_6NCl_{18}]$. The interaction of niobium with bromine in the presence of sodium bromide and tungsten at 720 °C yielded compound $Na[W_6OBr_{18}]$ that was unstable in air [58].

The authors of [59] studied the substitution of apical ligands in $[W_6CCl_{18}]^{2-}$. The interaction of $(Bu_4N)_2[W_6CCl_{18}]$ with CF_3SO_3H at 100 °C for 8 h yielded a black solution from which compound $(Bu_4N)_2[W_6CCl_{12}(CF_3SO_3)_6]$ was isolated. The reduction of this compound using two equivalents of Cp_2Co in DMF resulted in the substitution of terminal ligands to

form the cluster cation $[W_6CCl_{12}(DMF)_6]^{2+}$ isolated in the form of compounds $[W_6CCl_{12}(DMF)_6](BF_4)_2 \cdot DMF$. The interaction of $[W_6CCl_{12}(CF_3SO_3)_6]^{2-}$ with pyridine yielded pyridine-substituted cluster cation $[W_6CCl_{12}(py)_6]^{2+}$.

Group 7. For manganese, there are no known compounds with an interstitial atom whose Mn–Mn bond lengths and the number of bonding electrons would unambiguously allow classifying them as clusters. However, there are several examples of polynuclear complexes whose Mn–Mn distance is shorter than the sum of the Van der Waals radii, and there is a heteroatom in the center of the polyhedron formed by the metal atoms. These compounds are almost always stabilized by polydentate ligands. For example, the use of the hexadentate ligand $MeC(CH_2N(C_6H_4\text{-}o\text{-}NH))_3^{6-} = {}^{H}L$ allowed obtaining octahedral cluster complexes Mn(II) and Mn(III) with interstitial atoms N and O [60]. The reaction of the triangular cluster $({}^{H}L)Mn_3(THF)_3$ with pyridine oxide or PhIO in CH_3CN yielded compounds with the formula $[({}^{H}L)_2Mn_6(\mu_6\text{-}O)(NCMe)_4]$, and the reaction with $(Bu_4N)N_3$ resulted in $[({}^{H}L)_2Mn_6(\mu_6\text{-}N)](NBu_4)_2$. The oxidation of the latter by one equivalent of iodine in CH_3CN yielded $[({}^{H}L)_2Mn_6(\mu_6\text{-}N)(NCMe)_4]$ whose structure is identical to that of its oxygen containing analogue. The average Mn–Mn distance in these compounds is equal to 3.1 Å and substantially exceeds the typical length of covalent bonds Mn–Mn (2.8 Å).

For rhenium, there is only one type of clusters with an interstitial carbon heteroatom: bioctahedral cluster complexes with the $\{Re_{12}(\mu_6\text{-}C)(\mu_3\text{-}S)_{14}(\mu\text{-}L)_3\}$ core. The stability of this core allowed developing the chemistry of ligand substitution and to obtain a large number of other bioctahedral rhenium cluster complexes. The $K_8[Re_{12}CS_{17}(CN)_6]$ crystals are black and are formed with a high yield by the interaction of ReS_2 with the melt of KCN at 750 °C [61]. This salt is insoluble in deaerated water and in organic solvents; however, it is soluble in the form of anion $[Re_{12}CS_{17}(CN)_6]^{6-} \equiv [Re_{12}(\mu_6\text{-}C)(\mu_3\text{-}S)_{14}(\mu\text{-}S)(CN)_6]^{6-}$ as a result of oxidation. This anion contains 46 CSEs corresponding to two 23-electron fragments Re_6. The fact that the salts of this anion $K_6[Re_{12}CS_{17}(CN)_6]\cdot 20H_2O$ and $Cs_6[Re_{12}CS_{17}(CN)_6]$ are diamagnetic confirms the electron exchange and the existence of a common electronic structure in the Re_{12} fragment [62].

In the cluster anion $[Re_{12}CS_{17}(CN)_6]^{6-}$, there are two types of ligands that can act as reaction centers: terminal ligands CN^- and bridging ligands $(\mu\text{-}S)^{2-}$. The substitution of the cyanide ligands of anion $[Re_{12}CS_{17}(CN)_6]^{6-}$ was conducted by melting the salt $K_6[Re_{12}CS_{17}(CN)_6]\cdot 20H_2O$ with KOH at 320 °C. The resulting hydroxo complex was crystallized from water in the form of a crystallohydrate $K_6[Re_{12}CS_{17}(OH)_6]\cdot 4H_2O$ [63].

Some of the later studies were devoted to the protonation of terminal hydroxo groups in the anion $[Re_{12}CS_{17}(OH)_6]^{6-}$ and their substitution by other ligands: SO_3^{2-}, Cl^-, Br^- [63, 64]. The dehydration of $[Re_{12}CS_{17}(H_2O)_6]\cdot 4H_2O$ [65] in dynamic vacuum at 250 °C yielded black powder with the composition $Re_{12}CS_{17}$. This compound is a ternary cluster phase with a polymeric structure due to strong intermolecular contacts Re···S similar to such contacts in polymeric ternary phases $Re_6S_8Cl_2$ and $Re_6S_8Br_2$ and Mo···S contacts in the Chevrel phase Mo_6S_8 [66].

The phase $Re_{12}CS_{17}$ slowly dissolves in DMF in the presence of Et_4NBr to form $(Et_4N)_4(Me_2NH_2)_2[Re_{12}CS_{17}Br_6]$ [67]. The average Re–Br bond length is 2.547(9) Å, in good agreement with the bond lengths in octahedral rhenium clusters with terminal ligands Br^-. The anions $[Re_{12}CS_{17}X_6]^{6-}$ (X = Cl, Br) in solvothermal conditions in the presence of DMF undergo a two-electron reduction to $[Re_{12}CS_{17}X_6]^{8-}$; these anions contain 48 CSEs.

The internal ligands of bioctahedral rhenium clusters $(\mu\text{-}S)^{2-}$ also demonstrate chemical transformations. The interaction of solution $K_6[Re_{12}CS_{17}(CN)_6]\cdot 20H_2O$ with H_2O_2 in an alkaline medium changed its color from brown to purple due to the formation of the cluster anion $[Re_{12}CS_{14}(\mu\text{-}SO_2)_3(CN)_6]^{6-}$ [68]. The reaction proceeds selectively without affecting other ligands of the cluster (μ_3-S and CN) and without changing the number of CSEs. Ligands $(\mu\text{-}SO_2)^{2-}$ are significantly more reactive than ligands $(\mu\text{-}S)^{2-}$. It was shown that irradiating an aqueous solution of salt $K_6[Re_{12}CS_{14}(\mu\text{-}SO_2)_3(CN)_6]$ by light in a wide range of wavelengths in the presence of air oxygen leads to further oxidation of $\mu\text{-}SO_2$ groups and the formation of the cluster anion $[Re_{12}CS_{14}(\mu\text{-}SO_2)_2(\mu\text{-}SO_3)(CN)_6]^{6-}$. This anion was isolated and investigated structurally in the composition of salt $[Cu(NH_3)_5]_{2.6}[Re_{12}CS_{14}(SO_2)_3(CN)_6]_{0.6}[\{Re_{12}CS_{14}(SO_2)_2(SO_3)(CN)_5(\mu\text{-}CN)\}\{Cu(NH_3)_4\}]_{0.4}\cdot 5H_2O$. A mixed composition of the salt with respect to the anion indicates that the oxidation stage does not proceed quantitatively;

the resulting clusters decompose upon long exposure. In the CH_3CN solution, anion $[Re_{12}CS_{14}(\mu\text{-}SO_2)_3(CN)_6]^{6-}$ is oxidized in a more complex way leading to the simultaneous formation of products containing from one to three ligands $(\mu\text{-}SO_3)^{2-}$ [69]. It was shown that ligands $(\mu\text{-}SO_2)^{2-}$ can be also reduced to ligands $(\mu\text{-}S)^{2-}$ upon the action of sulfide and selenide anions in aqueous solutions. It was established by mass spectrometry that the reduction yields a number of intermediates, including clusters with ligands $(\mu\text{-}SO)^{2-}$. Two intermediates, $[Re_{12}CS_{14}(\mu\text{-}SO_2)_2(\mu\text{-}S)(CN)_6]^{6-}$ and $[Re_{12}CS_{14}(\mu\text{-}SO_2)(\mu\text{-}S)_2(CN)_6]^{6-}$, are isolated in the form of crystalline salts [69, 70]. Heating the salts of the cluster anion $[Re_{12}CS_{14}(\mu\text{-}SO_2)_3(CN)_6]^{6-}$ with KOH or KSeCN in the presence of small amounts of water led to the substitution of ligand $(\mu\text{-}SO_2)^{2-}$ by $\mu\text{-}O^{2-}$ or $\mu\text{-}Se^{2-}$, respectively, to form the salts of anions $[Re_{12}CS_{14}(\mu\text{-}O)_3(CN)_6]^{6-}$ and $[Re_{12}CS_{14}(\mu\text{-}Se)_3(CN)_6]^{6-}$ [71]. In the first case, the air oxygen was used as the source of ligand $(\mu\text{-}O)^{2-}$. To study the mechanism of this reaction, the interaction of salt $K_6[Re_{12}CS_{14}(\mu\text{-}SO_2)_3(CN)_6]$ with O_2 was investigated in thermogravimetry conditions by mass spectrometry detection of gaseous reaction products. Two possible reaction pathways were established. The first one is the oxidation of ligand $(\mu\text{-}SO_2)^{2-}$ to $(\mu\text{-}SO_3)^{2-}$ and then to anion SO_4^{2-} (HSO_4^- in an alkaline medium) and the elimination of the latter. The second one is the intramolecular two-electron oxidation of ligand $(\mu\text{-}SO_2)^{2-}$, the removal of gaseous SO_2 from the reaction zone, and the attachment of anion O^{2-} (formed by the two-electron reduction of air O_2) to vacant coordination positions of rhenium. A characteristic feature of this reaction is that it proceeds under soft conditions. The temperature increase during the reaction between $[Re_{12}CS_{14}(\mu\text{-}SO_2)_3(CN)_6]^{6-}$ and O_2/KOH up to 220 °C led to the replacement of both bridging ligands and terminal CN groups to form the $[Re_{12}CS_{14}(\mu\text{-}O)_3(OH)_6]^{6-}$ cluster anion.

The reaction of aqueous $[Re_{12}CS_{14}(\mu\text{-}O)_3(OH)_6]^{6-}$ with hydrohalic acids led to the formation of X-ray amorphous poorly soluble precipitates which are reduced in DMF in the presence of Et_4NCl or Et_4NBr to form new cluster anions $[Re_{12}CS_{14}(\mu\text{-}Cl)_3Cl_6]^{5-}$, $[Re_{12}CS_{14}(\mu\text{-}Br)_3Cl_6]^{5-}$, and $[Re_{12}CS_{14}(\mu\text{-}Br)_3Br_6]^{5-}$ [72]. The compounds based on these 48-electron anions were the first bioctahedral clusters exhibiting luminescent properties.

Similarly to many other transition metal cyano complexes [73-75], anionic complexes $[Re_{12}CS_{17}(CN)_6]^{6-}$ can coordinate to transition metal cations to form coordination polymers [76, 77].

TYPES OF STRUCTURES AND STRUCTURAL FEATURES OF CLUSTERS WITH INTERSTITIAL ATOMS

Types of the central atom environment (polyhedron). A significant number of examples of cluster compounds with interstitial atoms belong to one of the following three types of environments of the introduced atom: tetrahedron, octahedron, and triangular prism (Fig. 2).

The geometry of these polyhedra imposes rather strict restrictions on the ratios of metal–metal and metal–ligand bond lengths

$$\text{in the tetrahedron: } d(Z\text{—}M) = \frac{d(M\text{—}M)\cdot\sqrt{6}}{4} \approx 0.612\, d(M\text{—}M),$$

$$\text{in the octahedron: } d(Z\text{—}M) = \frac{d(M\text{—}M)\cdot\sqrt{2}}{2} \approx 0.707\, d(M\text{—}M),$$

where $d(M–M)$ is the distance between the metal atoms in the cluster; $d(Z–M)$ is the distance between the metal atoms and the interstitial atom.

For the metals in question, the typical metal–ligand bond lengths fall within the region of 1.95-2.00 Å for period 2 atoms and exceed 2.5 Å for period 3 atoms to result in quite long metal–metal distances in the octahedron and even longer

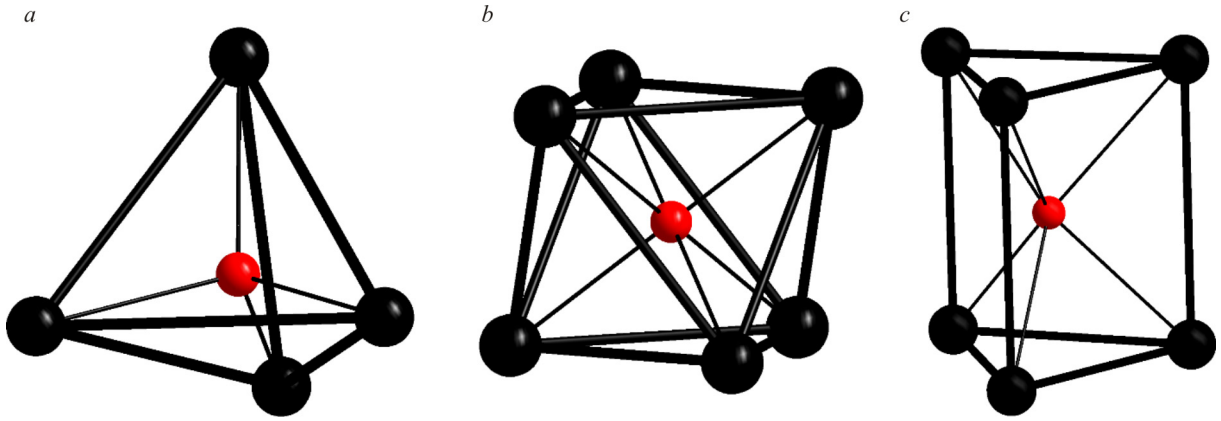

Fig. 2. Types of environments of the interstitial atom in the cluster compounds: tetrahedron (*a*); octahedron (*b*); trigonal prism (*c*).

distances in the tetrahedron. These metal–metal distances (3.0-3.3 Å) correspond to the bond order smaller than 1. In the trigonal prism, the ratio of metal–ligand and metal–metal bond lengths is more complicated and depends both on the distances between the metal atoms in the triangle M_3 and on the distances between the triangles in the prism:

$$d(Z—M) = \sqrt{\frac{d_1^2(M—M)}{3} + \frac{d_2^2(M—M)}{4}},$$

where $d(Z–M)$ is the distance between the metal atoms and the interstitial atom; $d_1(M–M)$ is the distance between the metal atoms in the triangle M_3 (shorter one); $d_2(M–M)$ is the distance between the metal atoms between the triangles M_3 (longer one).

The presence of longer bonds between triangles M_3 allows including large anions such as S^{2-} and Se^{2-} in the trigonal prismatic environment.

Tetrahedral environment of the interstitial atom (CN=4). Small number of known tetrahedral clusters is explained by steric restrictions imposed on the interatomic distances in tetrahedral clusters with an interstitial heteroatom. For niobium and tantalum, cyanocomplexes $[M_4OTe_4(CN)_{12}]^{6-}$ (M = Nb, Ta) containing the $M_4(\mu_4\text{-O})(\mu_3\text{-Te})_4$ cluster core with an interstitial oxygen atom [78, 79] were structurally characterized. The CSE number in these clusters is 4 and the $M–M$ distances are much longer than those in the corresponding metals or compounds with a single $M–M$ bond.

Tetrahedral clusters $\{ZLn_4\}$ are found among REM cluster complexes. To form the clusters, the REM atom should appear in the oxidation state 2+ or smaller. In this case, when one f electron jumps to the d orbital ($6s^05d^04f^n \rightarrow 6s^05d^14f^{n-1}$), this electron can be used in the intra-cluster bonding. One such example is compound Yb_4OCl_6 whose main fragment is an almost regular tetrahedron $(Yb^{2+})_4$ centered by the ligand O^{2-} and surrounded by 18 ligands Cl^-: three μ_3 bridging ligands, six μ_2 bridging ligands, and nine terminal ligands Cl^- (Fig. 3) [80]. The Yb–O distances are 2.243(3) Å and 2.287(1) Å; the average distance Yb–Yb in the tetrahedron is 3.879 Å. The authors of [81] obtained tetrahedral lanthanide complexes of other compositions containing REM atoms both in 2+ and 3+ oxidation states, e.g. lanthanum bromide $\{ZLa_4\}Br_7$ (Z = O, N). The structure of this compound is similar to that of $\{OLn_4\}X_6$; its bromide ions are bridges between the cluster complexes and are similar in two- or three-cluster complexes. The La–Z and La–La distances fall within the regions of 2.363(7)-2.453(11) Å and 3.725(1)-3.970(1) Å, respectively.

Five-nuclear complexes with an interstitial atom (CN = 5). There are several known examples of five-nuclear REM clusters forming trigonal bipyramidal clusters $\{ZLn_5\}$. In these clusters, two tetrahedra with a common face form a triangular bipyramid. The compound with the composition $Rb[\{C_2Pr_5\}Cl_{10}]$ (where this rare type of clusters was first discovered) contains an ethanide group C_2^{6-} that centers two tetrahedra and is located along the third-order axis (Fig. 4) [82]. The cluster anions are connected by bridging chloride ligands into a 3D framework $[\{C_2Pr_5\}Cl^{i-a}_{9/2}Cl^{a-i}_{9/2}Cl^{a-a-a}_{3/3}Cl^{a}_{3/3}]^-$. There are a number of compounds with formulas $A[\{C_2R_5\}X_{10}]$ and $[\{C_2Ln_5\}X_9]$ (A = K, Rb; Ln = La, Ce, Pr, Nd, X = Cl, Br, I)

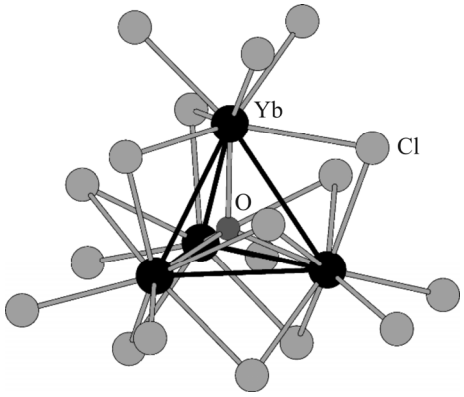

Fig. 3. Tetrahedron with an interstitial atom in the Yb_4OCl_6 structure.

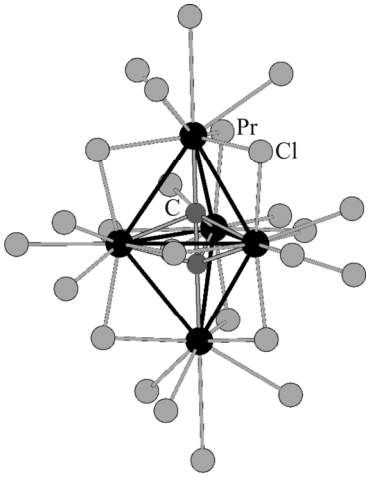

Fig. 4. Structure of the cluster in the $Rb[\{C_2Pr_5\}Cl_{10}]$ structure.

[82-85]. In all these compounds, the C–C distance corresponds to the single bonding so that anion C_2^{6-} can be represented as an ethanide unit providing six electrons for intra-cluster bonding, mainly due to C–Ln interactions. All these compounds contain 12 CSEs.

In the $H_4Zr_5Cl_{12}(PR_3)_5$ structure, atoms Zr form a distorted square pyramid with two long basal (3.41-3.54 Å) and two short (3.20-3.31 Å) edges. All eight Zr–Zr edges are coordinated by bridging chlorine atoms. According to the structural data, two hydrogen atoms are located along the Zr–Zr edges and two other hydrogen atoms are located in the center of triangular faces Zr_3 with longer basal edges [15].

Octahedral environment of the interstitial atom (CN = 6). Definitely, REM and zirconium clusters are the two largest groups of clusters with interstitial atoms in octahedral surroundings. REM ions have too little electrons to form metal–metal bonds required for clustering. Almost all REM clusters $\{M_6X_{12}\}$ contain interstitial atoms such as H, B, C, dimer unit C_2 (which gives four C_2^{4-} or six C_2^{6-} electrons), N, as well as transition metals (Cr–Zn, Ru–Pd, W–Au) to compensate the lack of electrons.

Isolated octahedral clusters are rarely met. One such example is compound $Cs_2Lu[\{CLu_6\}Cl_{18}]$ where both the cluster $\{CLu_6\}$ and the whole cluster complex $[\{CLu_6\}Cl_{18}]^{5-}$ are isolated [86]. The cluster complexes are connected by the seventh Lu atom surrounded by six Cl atoms. The largest families of isolated clusters are compounds of types 7-12 and 6-10, halides with the composition $Ln\{ZLn_6\}X_{12}$ and $\{ZLn_6\}X_{10}$ (e.g., see [87-89]). The most common stoichiometry is ZLn_7X_{12}, which can actually be represented as $Ln^{3+}[\{ZLn_6\}X_{12}]$, since it contains isolated cations Ln^{3+}. Such complexes are known for

most lanthanides with X = Cl, Br, I. The interstitial atom Z may be represented by most transition metals of groups 7-11 and by a series of non-transition elements B, C, N. These octahedral clusters are almost always distorted. All interstitial atoms Z have a higher electron affinity than the REM atoms in the clusters, and the Z–M bonds have a greater contribution to the cluster stability than the M–M bonds which are quite weak due to long bond lengths (3.8-3.9 Å). The intercluster bonding in ZLn_7X_{12} phases belongs to the $[ZLn_6X^{i}_{6}X^{i-a}_{6/2}X^{a-i}_{6/2}]$ type. Additional Ln^{3+} ions are located between the clusters in a distorted trigonal-antiprismatic environment formed only by the halogen atoms connecting the edges of two opposite faces of the cluster.

For the ratio Ln/X = 6/10, there are many cluster phases including B, C, C_2, Mn, Fe, Co, Ni, Cu, Ru, Rh, Pd, Re, Os, Ir, Pt, and Au as interstitial atoms. The RuY_6I_{10} structure (Fig. 5) shows how rare earth clusters counteract the lower halogen content while preserving the cluster fragments $\{Ln_6(Z)X_{12}\}$ [87].

Zirconium cluster complexes with an interstitial atom encompass a large group of halide octahedral clusters [90-93]. The formula of the discrete cluster fragment can be written as $[(Zr_6ZX^{i}_{12})X^{a}_{6}]^{m-}$ (X = Cl, Br, I; Z is the atom interstitial in the cavity of the octahedral metal core Zr_6; X^{i} is the bridging (inner) halogen atom located on one of the 12 octahedron's edges; X^{a} is the terminal halogen atom; the ligands are designated according to Schäfer's notation [10]). The structure of the cluster fragment $[(Zr_6ZX^{i}_{12})X^{a}_{6}]^{m-}$ is shown in Fig. 6.

There are known octahedral zirconium clusters where the interstitial atoms are represented by H, Be…N, Al…P, Ge, Cr…Ni. Such coordination environment is characteristic of all phases containing zirconium clusters; however, the Zr_6/X_{18} ratio is often not met in polymeric phases. As it was mentioned in the section devoted to the synthesis methods, zirconium clusters are obtained mainly by high-temperature solid-phase synthesis from binary compounds (e.g., zirconium and alkali metal halides) and simple substances [93]. High-temperature synthesis often leads to the formation of polymer compounds where the polymerization of cluster fragments is achieved due to the halide bridges connecting the neighboring cluster fragments. Thus, the number of common halide ligands increases while the number of halogen atoms per one Zr_6 fragment decreases as the degree of polymerization of cluster fragments in the solid phase increases. The general formula of cluster octahedral zirconium compounds existing in the solid phase can be written as $M_m[(Zr_6ZX_{12})X_n]$ (X = Cl, Br, I; $0 \le n \le 6$, M is an alkali metal cation or an alkaline earth metal cation). The fact that various polymer frameworks can be formed using

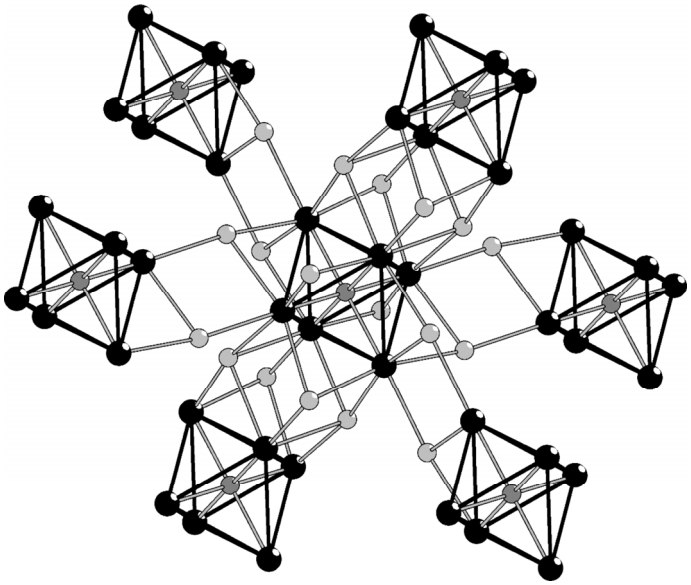

Fig. 5. Interaction of cluster fragments RuY_6I_{18} in the RuY_6I_{10} structure. Some iodine atoms are not shown.

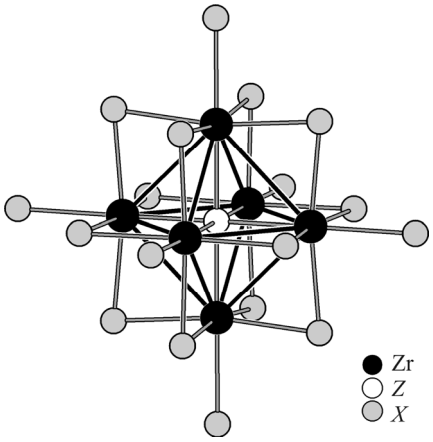

Fig. 6. Structure of the cluster fragment $[(Zr_6ZX^{i}_{12})X^{a}_{6}]^{m-}$.

TABLE 1. Examples of Cluster Complexes with the Zr_6ZX_{12} Core (X = Cl, Br, I) and Various Interstitial Heteroatoms Z

Z	Examples	CSEs
H	$[Zr_6HCl_{12}]$, $Li_6[(Zr_6HCl_{12})Cl_6]$	13
Be	$[Zr_6BeCl_{12}]$, $K[(Zr_6BeHal_{12})Hal]$ (Hal = Cl, Br), $K_3[(Zr_6BeCl_{12})Cl_3]$, $M_4[(Zr_6BeCl_{12})Cl_4]$ (M = Na, Cs)	14
B	$[Zr_6BBr_{12}]$, $[Zr_6BI_{12}]$ $(K,Cs)[(Zr_6BI_{12})I_2]$, $(K–Cs)_2[(Zr_6BCl_{12})Cl_3]$, $Rb_5[(Zr_6BCl_{12})Cl_6]$ $[(Zr_6BCl_{12})Cl_2]$	15 14 13
C	$[Zr_6CI_{12}]$ $(K,Rb,Cs)[(Zr_6CI_{12})I_2]$, $Cs_3[(Zr_6CCl_{12})Cl_4]$ $[(Zr_6CHal_{12})Hal_2]$ (Hal = Cl, Br, I), $Rb_4[(Zr_6CCl_{12})Cl_6]$, $M[(Zr_6CCl_{12})Cl_3]$ (M = K, Rb, Cs)	16 15 14
N	$[(Zr_6NCl_{12})Cl_3]$	14
Al	$Cs_{0.7}[(Zr_6AlI_{12})I_2]$	14/13
Si	$Cs_{0.3}[(Zr_6SiI_{12})I_2]$ $[(Zr_6SiI_{12})I_2]$	15/14 14
Ge	$[(Zr_6GeI_{12})I_2]$	14
P	$[(Zr_6PI_{12})I_2]$, $M_x[(Zr_6PI_{12})I_2]$ (M = Cs; x = 0.35; M = Rb, x not specified)	16/15
Cr	$[Zr_6CrI_{12}]$	18
Mn	$[Zr_6MnI_{12}]$ $Cs[(Zr_6MnI_{12})I_2]$, $Li_2[(Zr_6MnCl_{12})Cl_3]$	19 18
Fe	$[(Zr_6FeI_{12})I_2]$, $Li[(Zr_6FeI_{12})I_3]$, $Cs_{0.63}[(Zr_6\ FeCl_{12})Cl_3]$	18
Co	$Cs[(Zr_6CoI_{12})I_2]$, $[(Zr_6CoCl_{12})Cl_3]$	19/18
Ni	$[(Zr_6NiCl_{12})Cl_3]$	19

different polymerization methods is one possible reason for the existence of a large number of currently known phases $M_m[(Zr_6ZX_{12})X_n]$. Table 1 lists some examples of cluster complexes with the Zr_6ZX_{12} core (X = Cl, Br, I) and various interstitial heteroatoms Z.

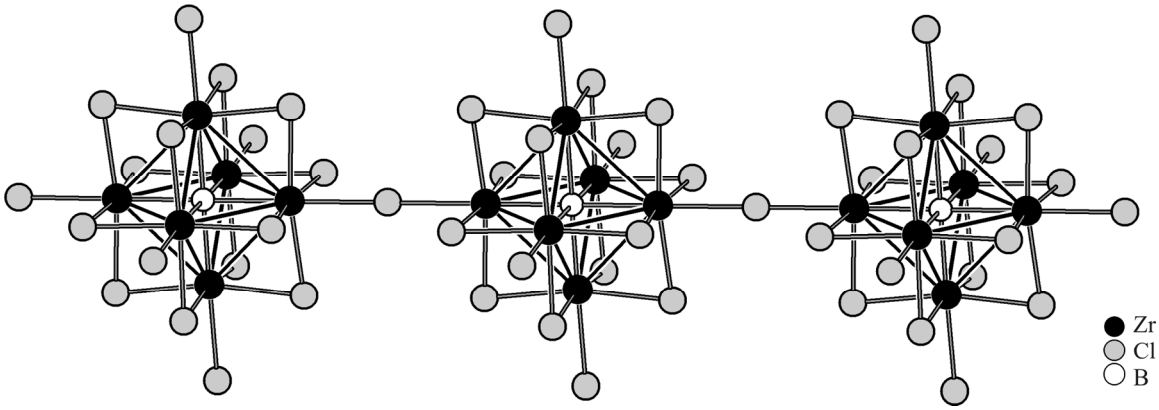

Fig. 7. Structure of the polymer chain $[Zr_6BCl_{17}]_n^{4n-}$.

The above bonding principles can be illustrated by the example of several compounds having different stoichiometries. The Zr_6ZX_{17} stoichiometry occurs in the structure of compounds $Ba_2[Zr_6BCl_{17}] = Ba_2[(Zr_6BCl_{12}^{i})Cl_4^{a}Cl_{2/2}^{a-a}]$ [94]. The cluster anions $[Zr_6BCl_{17}]^{4-}$ in the crystal structure of this compound are bonded to each other by bridging chlorine atoms occurring in *trans* positions to form an infinite chain directed along the crystallographic axis *c* (Fig. 7). The cations are located in the space between the anion chains.

The stoichiometry Zr_6ZX_{16} is achieved in the structure of compounds $Cs_3[Zr_6CCl_{16}]=Cs_3[(Zr_6CCl_{12})Cl_2^{a}Cl_{4/2}^{a-a}]$ [95]. Each cluster fragment $[Zr_6CCl_{18}]$ is coordinated to four neighboring clusters via four terminal chloride ligands Cl^{a-a} lying in the same plane. This kind of coordination leads to the formation of a layered structure (Fig. 8). Cations Cs^+ are located in the interlayer space.

The stoichiometry Zr_6ZX_{15} is achieved in the structure of compounds $K_2[Zr_6CCl_{15}]=K_2[(Zr_6CCl_{12}^{i})Cl_{6/2}^{a-a}]$ [96]. Each terminal chlorine atom belongs simultaneously to two cluster cores. The resulting 3D framework in the cross-section by the *ab* plane is shown in Fig. 9.

The stoichiometry Zr_6ZX_{14} is achieved in the structure of compounds $Zr_6CI_{14} = [(Zr_6CI_{10}^{i}I_{2/2}^{i-a}I_{2/2}^{a-i})I_{4/2}^{a-a}]$ [97]. In this case, the Zr/*X* ratio smaller than 6/15 cannot be achieved only due to the collectivization of all terminal ligands *X*; therefore, the polymerization occurs also via the inner ligands. Fig. 10 shows the coordination environment of one of the cluster fragments in the resulting 3D framework. One special feature of this coordination is that $Zr–Cl^{i–a}$ distances are elongated: their length (~3.49 Å) is about 0.6 Å larger than covalent bonds $Zr–Cl^{i}$ (2.91 Å).

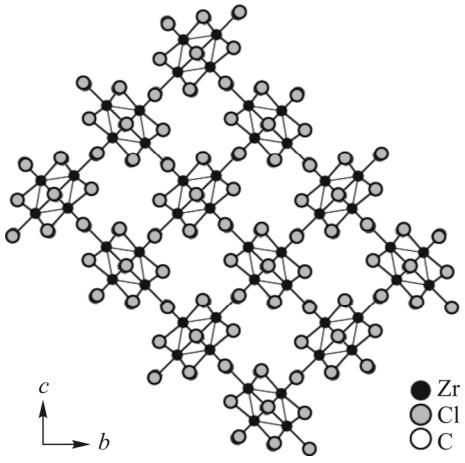

Fig. 8. Packing of cluster anions in compound $Cs_3[Zr_6CCl_{16}]$. View in the *bc* plane, cations Cs are not shown.

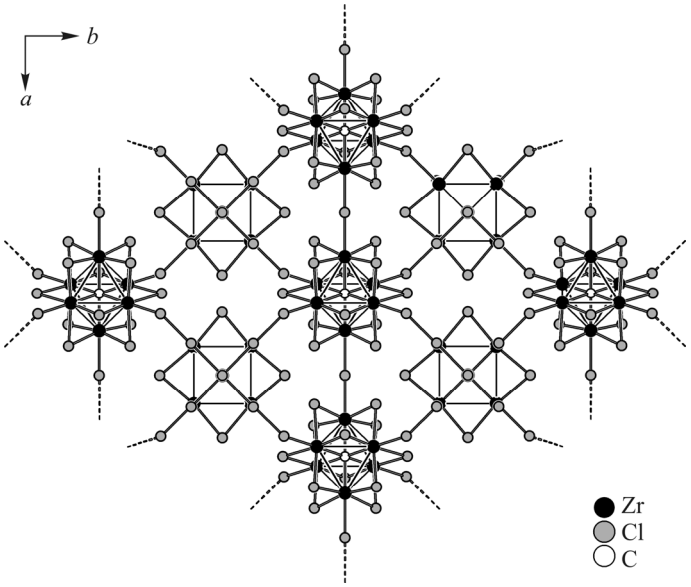

Fig. 9. Structure of the 3D framework $[Zr_6CCl_{15}]_n^{2n-}$ in compound $Rb_2[Zr_6CCl_{15}]$.

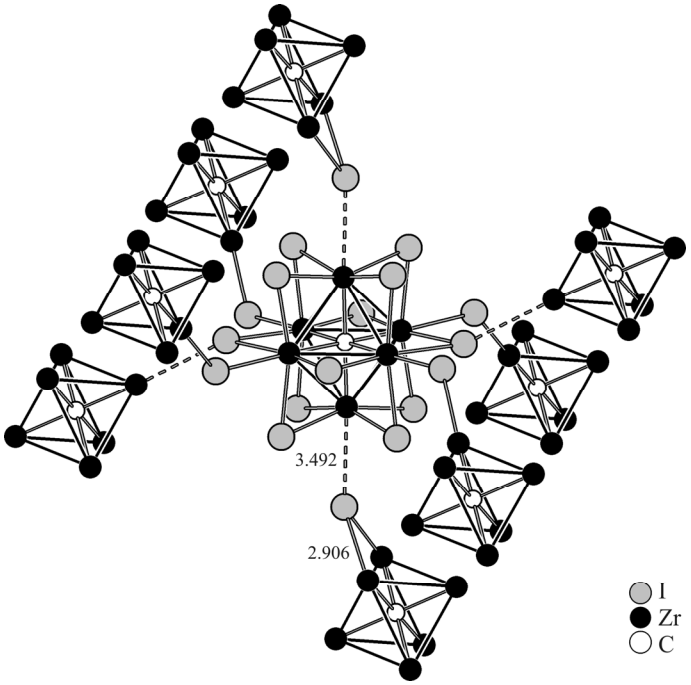

Fig. 10. Coordination environment of the cluster fragment in the structure of compound $[Zr_6CI_{14}]$. Some iodine atoms are not shown.

The stoichiometry Zr_6ZX_{12} is achieved in the structure of compounds $Zr_6CI_{12} = [(Zr_6CI_6^{i}I_{6/2}^{i-a}I_{6/2}^{a-i})]$. The Zr_6/X_{12} ratio is the minimum possible in the structure of solid cluster phases of zirconium. It is achieved by the collectivization of all terminal and a half of inner halide ligands to form a 3D framework that is close, in terms of space filling, to close-packings of equal spheres. The further increase in the degree of polymerization seems to be impossible in these systems due to steric hindrances.

Octahedral environment of the interstitial atom is less typical of other transition metals. Compounds $A[Hf_6ZC1_{14}]$ (A = Li, Na, K and Z = B, C) are crystallized in the Nb_6Cl_{14} structural type, while compounds $A[Hf_6ZC1_{15}]$ (A = K, Cs, Z = B,

C) are crystallized in the $CsK[Zr_6BCl_{15}]$ structural type; a non-stoichiometric compound $Na_{0.8}Hf_6(B)Cl_{15}$ is crystallized in the Ta_6C1_{15} structural type. The unit cell volumes of hafnium cluster phases are ~ 3% smaller than those in similar zirconium compounds. The average Hf–Hf distance in the structure of phase $Na_{0.8}[Hf_6ZC1_{15}]$ (tetragonal crystal system, space group $I4_1/acd$, $Z = 16$) is 3.206(4) Å, which is somewhat shorter than the average Zr–Zr distance in the isostructural phase $Na[Zr_6BCl_{15}]$ (3.245 Å) [39].

The structure of compounds $K[V_3Te_3O_{0.42}]$ consists of polymer chains $[V_6Te_6O_x]_\infty$ formed by condensed planar fragments V_3Te_3; a part of octahedral voids between these fragments is occupied by oxygen atoms (Fig. 11). The distances V–V and V–Te fall within the regions of 2.758(4)-2.789(5) Å and 2.760(4)-2.801(5) Å, respectively.

Prismatic environment of the interstitial atom (CN = 6). The formation of prismatic fragments around the interstitial atom is characteristic of group 5-7 elements. In the crystal structure $Rb_3[Nb_6SBr_{17}]$, 18 bridging bromine atoms are arranged around a trigonal-prismatic fragment $Nb_6\mu_6$-S (Fig. 12) [41].

The metal framework Nb_6 has a distorted trigonal-prismatic geometry. The average length of Nb–Nb bonds (the edges of triangular prism faces) is 2.97 Å, while the Nb···Nb distance between triangular faces reaches 3.28 Å. The quantum chemical calculations showed that the interactions of Nb atoms between the triangular faces are weak bonds formed mainly by Nb–μ_6-S bonds whose length is equal to 2.37 Å (see the section "Oligomers and infinite networks composed of clusters").

The crystal structure of compounds $[Nb_6SI_9]$ is composed of cluster fragments $[Nb_6I^i_6\ I^{a-a}_{6/2}S^{i-i}_{2/2}]$ with an octahedral metal core that are connected in a polymer chain by bridging atoms μ-I and μ_6-S (Fig. 13) [46]. The lengths of Nb–Nb bonds in the octahedron fall within the region of 2.802(2)-3.165(2) Å, and the shortest Nb–Nb distance between the edges of the

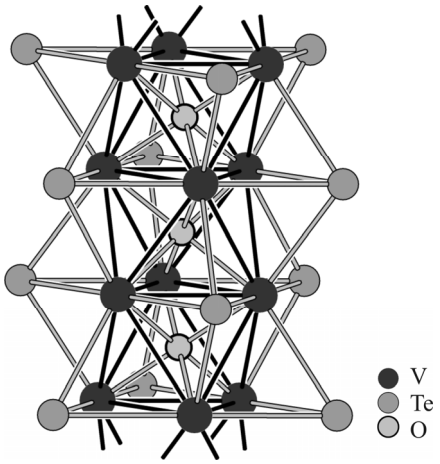

Fig. 11. Fragment of the polymer chain in the structure of compound $K[V_3Te_3O_{0.42}]$.

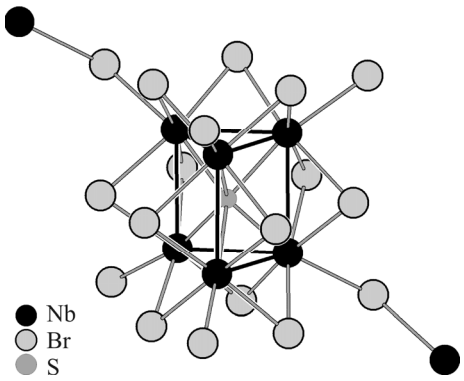

Fig. 12. Fragment of the polymeric chain in the structure of compound $Rb_3[Nb_6SBr_{17}]$.

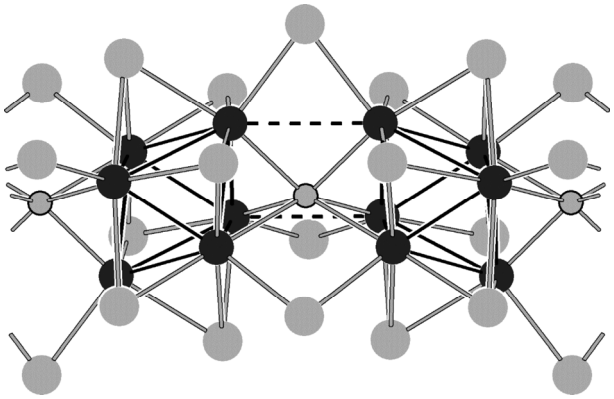

Fig. 13. Fragment of the polymer chain in the structure of compound $[Nb_6SI_9]$.

neighboring octahedra is equal to 3.358(2) Å. The lengths of Nb–I and Nb–(μ_6-S) bonds fall within the regions of 2.817(2)-2.916(2) Å and 2.408(5)-2.544(5) Å, respectively.

The reaction of compound $[Nb_6SI_9]$ containing 19 CSEs with an excess of H_2 at 400-550 °C lead to the formation of an isostructural 20-electron $[Nb_6(H)SI_9]$ with an interstitial hydrogen atom in the octahedral cavity of the metal core [46]. Structures $Mo_6I_6Se_8$ [50] and $BaMo_{12}S_{24}$ [49] demonstrate a similar type of bonding octahedra Mo_6, while the role of the ligands between the faces of the neighboring clusters is played by μ_6-Se and μ_6-S, respectively, to form a trigonal prismatic environment of heteroatoms.

In the trigonal-prismatic tungsten clusters with $[W_6ZCl_{12}]$ (Z = C, N) cores (Fig. 14), the metal core consisting of six tungsten atoms is centered by carbon or nitrogen atoms [51, 54, 55, 57, 59, 98-100]. In the structure of discrete $[W_6CCl_{18}]$, a bridging chloride ligand is coordinated to each W–W bond of the prism's triangular faces (their length is 2.743 Å), and two more such ligands are coordinated by each W–W bond of the prism's rectangular faces (2.930 Å) [51]. Also, one terminal chloride ligand K is coordinated to each atom W. In the layered polymer W_6CCl_{16}, fragments $[W_6CCl_{18}]$ are connected into a polymer network by Cl^{a-a} bridges so that the formula of these compounds can be written in Schäfer's notation as $[(W_6CCl_{12})Cl^a_2Cl^{a-a}_{4/2}]$. Prism W_6 is stretched along axis 3: the W–W bond lengths are equal to 2.636(4)-2.670(1) Å in the triangular faces and to 3.007(1)-3.045(1) Å in the rectangular faces. The structure of the 24-electron clustered anion $[W_6CCl_{18}]^{2-}$ in the molecular complex $(Bu_4N)_2[W_6CCl_{18}]$ is similar to that of the above $[W_6CCl_{18}]$. The W–W bond lengths are equal to 2.667 Å for the prism's triangular faces and to 3.028 Å for the rectangular faces.

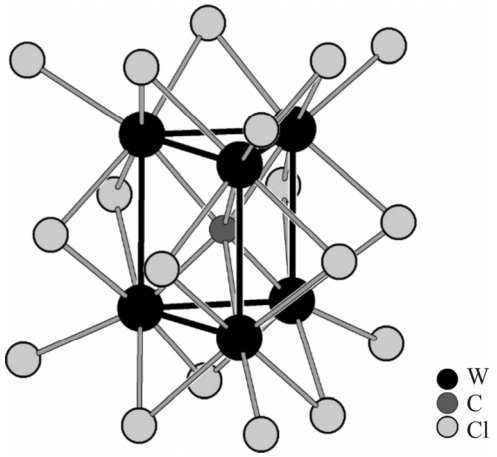

Fig. 14. Structure of the cluster complex $[W_6CCl_{18}]$.

TABLE 2. Average Bond Lengths in Trigonal Prismatic Tungsten Clusters. The Data Refer to the $[W_6CCl_{18}]^{n-}$ Anions in Compounds $(Bu_4N)[W_6CCl_{18}]$, $(Bu_4N)_2[W_6CCl_{18}]$, and $(Ph_4P)_3[W_6CCl_{18}]\cdot MeCN\cdot Et_2O$

Cluster	CSEs	W–W$^{\Delta}$, Å	W–W$^{\square}$, Å	W–Z, Å	W–Cl$^{i\Delta}$, Å
W_6CCl_{18}	14	2.743	2.930	2.157	2.361(2)
$[W_6CCl_{18}]^-$	15	2.74(1)	2.93(2)	2.157(8)	2.389(4)
W_6CCl_{16}	16	2.65(2)	3.03(2)	2.15(5)	2.389(7)
$[W_6CCl_{18}]^{2-}$	16	2.667	3.028	2.1595	2.381(5)
$[W_6NCl_{18}]^-$	16	2.6518	3.0705	2.1682	2.382(1)
W_6CCl_{15}	17	2.68	3.00	2.15(5)	2.38(2)
$[W_6CCl_{18}]^{3-}$	17	2.71(5)	2.96(8)	2.15(3)	2.412(8)
$[W_6NCl_{18}]^{2-}$	17	2.67(1)	3.07(1)	2.173(7)	2.397(5)
$[W_6NCl_{18}]^{3-}$	18	2.69(6)	3.0(1)	2.16(2)	2.408(13)
$[W_6OBr_{18}]^-$	17	2.7246(3)	3.0018(3)	2.17416(17)	2.6339(5)

The comparison of interatomic distances in the clusters shows (Table 2) that the deviation of the number of CSEs from 16 affects the W–W distances: removing or adding the electrons increases their number in the prism's triangular faces and decreases their number in the rectangular faces.

In the anion $[Re_{12}CS_{17}(CN)_6]^{8-}$, the metal core consists of two octahedral fragments $\{Re_6^{III}\}$ connected to each other by ligand $(\mu_6\text{-}C)^{4-}$ and three ligands $(\mu\text{-}S)^{2-}$ along the prism's face (Fig. 15) [61].

Thus, the structure of the clustered anion contains outer and inner faces of the octahedra. The latter, in turn, form the prismatic fragment $\{Re_3(\mu_6\text{-}C)(\mu\text{-}S)_3Re_3\}$ containing an interstitial carbon atom in its center. The coordination environment of rhenium atoms of the octahedral fragments is supplemented by the face ligands $(\mu_3\text{-}S)^{2-}$ and by the terminal ligands CN^- coordinated to the outer faces of the octahedra. The formal calculated number of valence electrons signifies that this cluster has 48 CSEs corresponding to 24 two-electron Re–Re bonds in two octahedral fragments while no Re–Re covalent bonding is formed in the central prismatic fragment. This assumption is confirmed by the Re–Re bond lengths. According to the XRD data, the average interatomic distance Re–Re in the $\{Re_6S_7C\}$ fragments are 2.595 Å and 2.591 Å for the atoms located on the outer and on the inner faces of the octahedra, respectively. These values are comparable to the bond lengths in the 24-

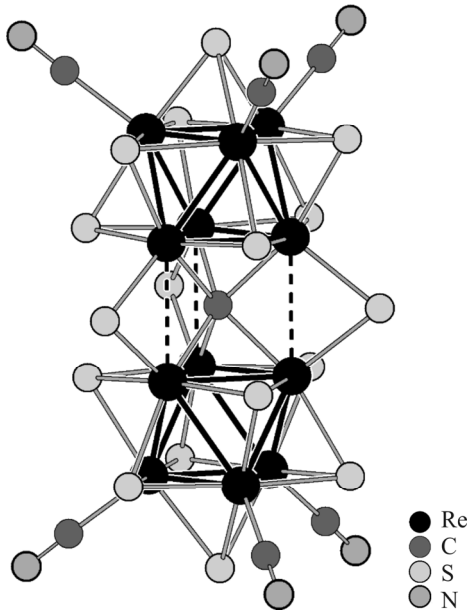

Fig. 15. Structure of the anionic complex $[Re_{12}CS_{17}(CN)_6]^{8-}$.

electron cluster anion $[Re_6S_8(CN)_6]^{4-}$ (2.599 Å) [101]. At the same time, the distances between the rhenium atoms from the neighboring octahedral fragments are equal to 3.168 Å.

Removing two valence electrons from the cluster orbitals significantly affects the interatomic distances in the crystal, and these differences mainly refer to the central fragment $\{Re_3(\mu_6\text{-}C)(\mu\text{-}S)_3Re_3\}$. Thus, the Re–Re bond lengths between rhenium atoms forming the "inner" faces of the octahedra became more than 0.1 Å longer to reach the average value of 2.692 Å. To the contrary, the distance between the rhenium atoms of the neighboring octahedral fragments became 0.267 Å shorter (2.901 Å as compared to 3.168 Å in the 48-electron cluster anion). Thus, the oxidation of the cluster significantly distorted the octahedral fragments $\{Re_6S_7C\}$ and decreased the distances between them.

Studying the structure of anions $[Re_{12}CS_{17}L_6]^{n-}$, L = OH, SO_3, Cl, Br showed that the substitution of terminal ligands had virtually no effect on the bond lengths inside the cluster core. Thus, the Re–Re distances in the $\{Re_6S_7C\}$ fragments are equal to 2.5914(10) Å for the outer faces of the octahedra and to 2.6888(9) Å for the inner faces while the Re…Re distance between the octahedra is 2.9124(12) Å. The Re–O bond length is 2.091(14) Å, in good agreement with the Re–O(OH) bond lengths reported for the octahedral cluster anion $[Re_6S_8(OH)_6]^{4-}$ [102].

At the same time, the geometry of octahedra $\{Re_6\}$ in the 48-electron anions $[Re_{12}CS_{14}(\mu\text{-}S)_3L_6]^{8-}$ (L = Cl, Br) is virtually not distorted, the average Re–Re bond lengths on the outer and inner faces are almost equal, and the Re…Re distances in the prismatic fragment $\{Re_3(\mu_6\text{-}C)(\mu\text{-}S)_3Re_3\}$ are equal to 3.170(3)-3.172(3) Å. Table 3 summarizes the interatomic distances in the twelve-nuclear rhenium cluster complexes with an interstitial carbon atom and various bridging ligands L in the prismatic fragment $\{Re_6(\mu_6\text{-}C)(\mu\text{-}L)_3\}$.

TABLE 3. Main Interatomic Distances in Twelve-Nuclear Rhenium Cluster Complexes with an Interstitial Atom Carbon and Various Bridging Ligands L in the Prismatic Fragment $\{Re_6(\mu_6\text{-}C)(\mu\text{-}L)_3\}$

Cluster anion	Re_{in}—Re_{out}	Re_{in}—Re_{out}	Re_{in}—Re_{out}	Re⋯Re (in the prism $\{Re_6C\}$)	Re–μ-L	Re–μ_6-C	Ref.
			46 CSEs				
$[Re_{12}CS_{14}(\mu\text{-}O)_3(CN)_6]^{6-}$	2.6725(6)-2.6746(8); 2.6732(8)	2.5924(7)-2.6017(8); 2.596(4)	2.6244(6)-2.6293(6); 2.627(2)	2.8263(11)-2.8368(8); 2.833(5)	2.004(10)-2.041(8); 2.02(2)	2.092(8)-2.102(2); 2.095(5)	[71]
$[Re_{12}CS_{14}(\mu\text{-}S)_3(CN)_6]^{6-}$	2.6919(6)	2.5983(7)	2.6255(5)	2.9133(8)	2.380(3)	2.1301(4)	[61]
$[Re_{12}CS_{14}(\mu\text{-}Se)_3(CN)_6]^{6-}$	2.6789(9)	2.5955(10)	2.6203(6)	2.9425(10)	2.497(2)	2.1346(5)	[71]
$[Re_{12}CS_{14}(\mu\text{-}SO_2)_3(CN)_6]^{6-}$	2.6396(6)-2.6563(7); 2.648(5)	2.5955(7)-2.6076(7); 2.601(4)	2.6040(6)-2.6253(6); 2.617(5)	2.9590(6)-2.9995(6); 2.98(2)	2.389(3)-2.429(3); 2.41(1)	2.118(10)-2.157(11); 2.14(2)	[68]
$[Re_{12}CS_{14}(\mu\text{-}SO_2)_2(\mu\text{-}SO_3)(CN)_6]^{6-}$	2.6508(8)-2.6643(8); 2.658(5)	2.5928(7)-2.6047(9); 2.598(4)	2.6066(7)-2.6214(8); 2.615(5)	2.9571(7)-3.0373(8); 2.99(4)	2.372(14)-2.459(15); 2.41(3) ($Re–S_{SO2}$); 2.397(10) ($Re–S_{SO3}$); 2.22(2) (Re–O)	2.116(14)-2.169(15); 2.14(2)	[68]
			48 CSEs				
$[Re_{12}CS_{14}(\mu\text{-}S)_3(CN)_6]^{8-}$	2.591	2.595	2.622	3.168	2.425	2.179	[61]
$[Re_{12}CS_{14}(\mu\text{-}Br)_3Cl_6]^{5-}$	2.555(2)	2.589(2)	2.577(2)-2.586(2); 2.582(5)	3.185(4)	2.564(4)	2.171(2)	[72]

Atoms Re_{out} and Re_{in} refer to the outer and inner faces of the octahedron $\{Re_6\}$ with respect to ligand μ_6-C.

Oligomers and infinite networks composed of clusters. In the above examples of clusters with interstitial atoms, the cluster complexes occur in the form of isolated fragments or are linked into polymer chains, networks, frameworks due to the collectivization of apical and/or inner ligands. Such compounds include the above complexes $[Nb_6SI_9]$, $Mo_6I_6Se_8$ [50], and $BaMo_{12}S_{24}$ [49] where octahedra M_6 are connected into infinite chains by μ_6-Z ligands.

The rich crystal chemistry of REM clusters includes examples of other compounds where the octahedra of the neighboring metal clusters Ln_6 have common edges giving rise to dimers, trimers, and more complex structures. For example, two octahedra with a common edge were found in the structure $Gd_5Cl_9C_2 = \{(C_2)_2Gd_{10}\}Cl_{18}$ [103]. In this structure (Fig. 16), the "dumbbells" C_2^{6-} act as the interstitial units while pieces $\{(C_2)_2R_{10}\}X_{26}$ are connected by halide bridges into a 3D network.

Two types of trimers are realized for REM clusters: open trimers, i.e. *trans–trans* connected trimers observed in $\{(C_2)_3R_{14}\}I_{20}$ for R = La, Ce, Pr (Fig. 17), and closed trimers observed in $\{Ir_3Gd_{11}\}Br_{15}$ [104].

For tetramers, there also two known types of structures containing a tetrameric fragment $\{Z_4Ln_{16}\}X_{36}$. The first type was described in compound $\{B_4Tb_{16}\}Br_{23}$ [105]: the boron atoms are located in the centers of the octahedra to form a rhombus with B–B distances equal to ~ 4 Å. In the second type of tetramers found in $\{Ru_4Y_{16}\}I_{20}$ [106], the interstitial Ru atoms form a tetrahedron.

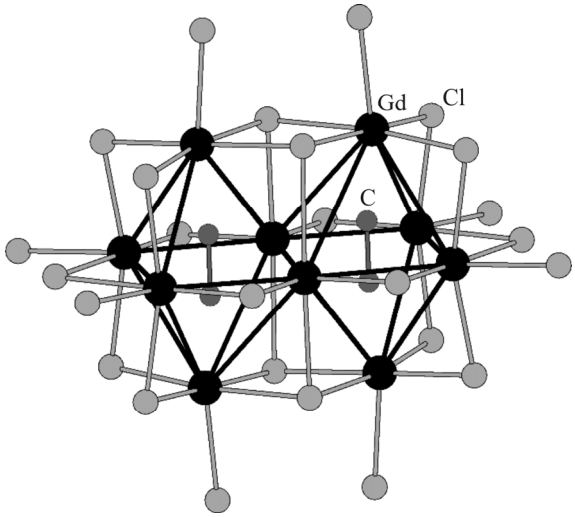

Fig. 16. Fragment of the $Gd_5Cl_9C_2=\{(C_2)_2Gd_{10}\}Cl_{18}$ structure.

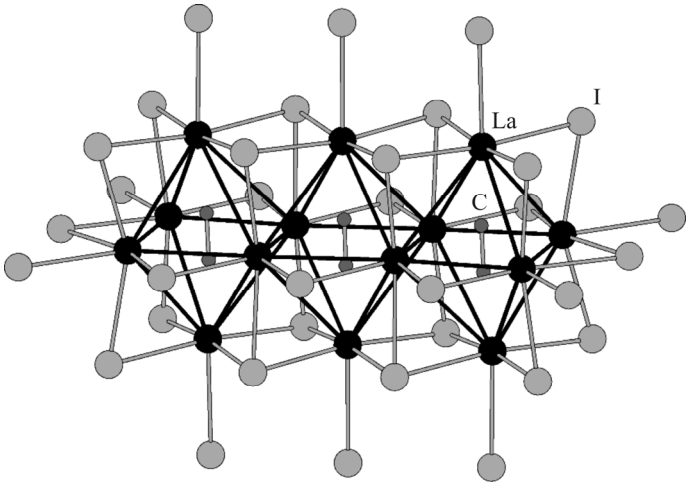

Fig. 17. Fragment of the $\{(C_2)_3La_{14}\}I_{20}$ structure.

The infinite expansion of dimers, *trans* trimers, and *trans–cis* tetramers leads to the formation of linear and zigzag chains. In all these cases, the octahedral clusters $\{ZLn_6\}$ are connected into chains by common edges, in agreement with the general formula $\{Z_xLn_{4x+2}\}$; the most condensed case corresponds to the composition $\{ZLn_4\}X_6$.

There are various degrees of condensation of single chains into even more condensed structures which can be grouped in three main families: $Ln_{2n+2}X^{i}_{2}X^{i-i}_{2/2}X^{i-a}_{2/2}X^{a-i}_{2/2}(Z)_n$ (*a*), $Ln_{2n-2}X^{i}_{2}X^{i}_{2n-2}X^{i-i}_{2/2}X^{i-a}_{2/2}X^{a-i}_{2/2}(Z)_n$ (*b*), and $Ln_4(C_2)X_5$ (*c*), where *n* corresponds to the number of condensed chains formed by octahedra $Ln_6(Z)$. Family *a* contains compounds Ln_4X_5Z ($n = 1$), $Ln_6X_7Z_2$ ($n = 2$) [107], and Ln_2X_2Z ($n = \infty$). The stoichiometry of family *b* coincides with that of family *a* for $n = 1$, with that of $Ln_6X_6Z_2$=Ln_3X_3Z for $n = 2$ [108], and corresponds to phases Ln_2XZ for $n = \infty$ [109]. The rhombic $Ln_4(C_2)Cl_5$ (Ln = La, Pr) and $Ln_4(C_2)Br_5$ (Ln = La, Ce) are the first members of family *c* where $n = 1$. The crystal chemical formula in these phases is described as $Ln_{2n-2}X^{i-i}_{2/2}X^{i-i}_{2n-2}X^{i-a}_{4/2}X^{a-i}_{4/2}(Z)_n$ i.e. all these halides are bridged [110-112].

ELECTRONIC STRUCTURE

The role of the interstitial heteroatom in the formation of the electronic structure of transition metal cluster complexes is of utmost importance. As it was mentioned in the section "Tetrahedral environment of the interstitial atom (CN = 4)", the number of known examples of such clusters is small; their electronic structure is virtually not known. The authors of [78] used the extended Hückel method to show that the degenerate HOMO orbitals in the $[NbOTe_4(CN)_{12}]^{6-}$ anion (formed mainly by niobium orbitals) are bonding in nature and contain no contribution of oxygen orbitals.

The electronic structure of compounds with octahedral and trigonal prismatic environments of the interstitial atom have been studied in more detail.

Interstitial atom in an octahedral environment. It is convenient to begin considering the electronic structure of octahedral transition metal cluster complexes with well-studied octahedral clusters with the composition M_6X_m (*X* is a halide ligand) and then pass on to the clusters with interstitial atoms. The splitting of valence $(n–1)d$ orbitals of metal atoms in the field of weak π donor halide ligands and the hybridization of obtained σ, π, and δ orbitals with *p* orbitals of the ligands leads to the formation of the bunches of bonding and antibonding molecular orbitals centered mainly on the metal atoms and, to a smaller extent, on the ligands. The number and symmetry of molecular orbitals are determined by the number of metal atoms in the cluster core, its geometry and symmetry, and are weakly dependent on the ligand type of the same geometry. Thus, group 6 and 7 metals are characterized by the formation of $[M_6(\mu_3\text{-}X_8)X_6]^n$ type clusters whose octahedral metal core is coordinated by its faces with eight bridging inner ligands. The calculation of the electronic structure of these clusters in the idealized symmetry O_h shows that the bunch of upper bonding orbitals includes 12 molecular orbitals with symmetries a_{1g}, t_{1u}, t_{2g}, t_{2u}, and e_g consisting mainly of *d* orbitals of metal atoms with a small contribution of *s* and *p* orbitals [87]. Therefore, 24 electrons are required to fill all metal-centered bonding orbitals, which is ensured by the d^4 configuration of metal atoms (Re^{3+}, Mo^{2+}). This electronic configuration is characteristic of electron-saturated clusters $\{Mo_6X_8\}^{4+}$ and $\{Re_6Q_8\}^{2+}$ (Q = S, Se, Te) (Fig. 18).

Group 4 and 5 metals form $[M_6(\mu\text{-}X_{12})X_6]^n$ type octahedral clusters with inner ligands coordinated along the edges of the octahedron of metal atoms. The electronic structure of such clusters (also calculated within the O_h symmetry) shows the presence of seven bonding metal-centered molecular orbitals with symmetries a_{1g}, t_{2g}, and t_{1u} (Fig. 19) [87]. The 14 valence electrons required to fill these orbitals form mixed d^2 and d^3 configurations for the metal atoms in the cluster core. The gap between the LUMO a_{2u} and the HOMO is quite large; however, this gap can be diminished due to the distortions in the cluster geometry so that orbital a_{2u} can accept two more electrons. Group 5 metals (Nb, Ta) readily form electron-saturated clusters with nuclei $\{M_6X_{12}\}^{2+}$ and $\{M_6X_{12}\}^{3+}$ (16 and 15 CSEs with formal oxidation states of metal atoms equal to 2.33 and 2.5, respectively). At the same time, all bonding metal-centered orbitals are not completely filled in similar clusters of group 4 and 3 metals. To compensate the lack of electrons in the *M–M* bonds, the heteroatoms always occur in the cavities of octahedral halide clusters of group 4 and 3 metals.

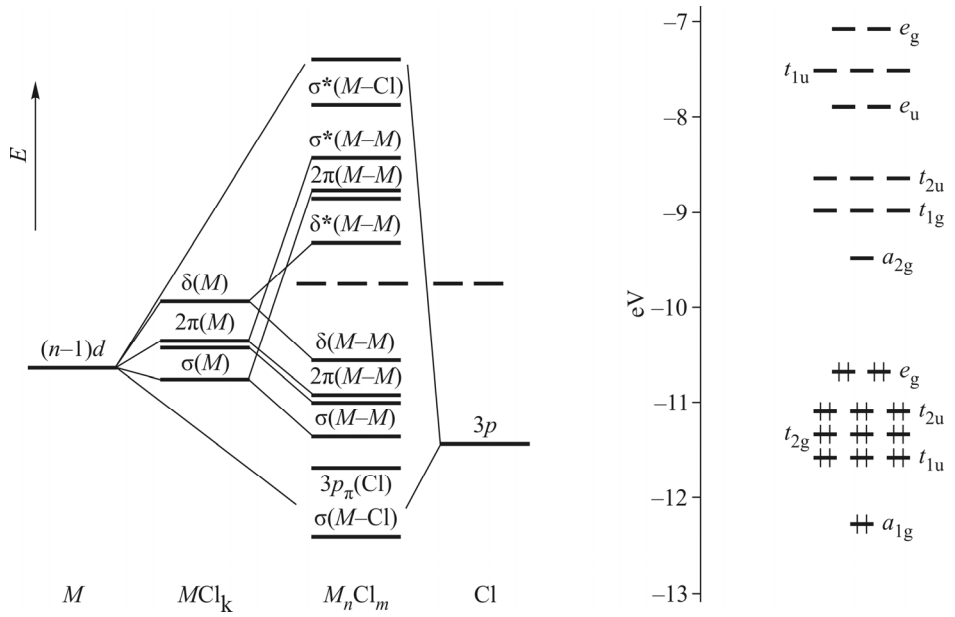

Fig. 18. Typical system of molecular orbitals of clusters $[M_6(\mu_3\text{-}X_8)X_6]^n$.

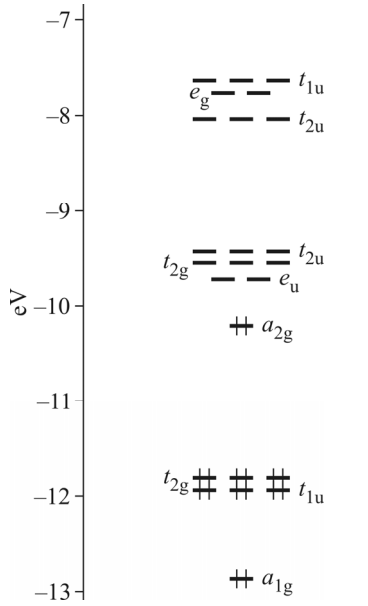

Fig. 19. Typical system of molecular orbitals of clusters $[M_6(\mu\text{-}X_{12})X_6]^n$.

Thus, introducing the heteroatom into the cluster metal core is due to the requirements for the cluster's electronic stability. The number of electrons available for the formation of metal–metal bonds decreases as the group number decreases or the transition metal's oxidation state increases so that a larger number of electrons donated by the ligands is required to fill the bonding orbitals of the transition metal polyhedron. The volume of space available for the ligands around the metal core is limited, and the discrete heteroatom can enter the inner cavity of the metal polyhedron while donating its valence electrons to bonding orbitals. Whereas the introduction of a heteroatom is almost imperative for the existence of clusters of group 3 and 4 metals, this phenomenon is less common for the metals from the groups with higher numbers and depends on the geometry and stoichiometry of the cluster.

Among discrete cluster compounds, the greatest variety of the types of interstitial heteroatoms is demonstrated by octahedral zirconium halide clusters with cores $\{Zr_6XCl_{12}\}$ (Table 1). Their metal cores can include atoms with different ionic radii and electronic configurations. In the case of *s*- or *p*-block elements, the cluster has an electronic structure with seven top metal-centered bonding and non-bonding orbitals with symmetries a_{1g}, t_{2g}, and t_{1u} which can be filled up by 14 CSEs. Since orbitals a_{1g} and t_{1u} have a significant portion of valence AOs from the interstitial atom, the latter can be considered as a donor of electrons for the bonding between the metal atoms. The gap between the LUMO a_{2u} and the HOMO is quite large; however, this gap can be diminished due to the distortions in the cluster geometry so that orbital a_{2u} can accept two more electrons. Therefore, the maximum number of electrons on the bonds in the metal octahedron reaches 16, as it was observed in the $\{Zr_6CI_{12}\}$ core [113]. When a *d*-block element is introduced inside the cavity, molecular orbitals a_{1g}, t_{2g}, and t_{1u} are complemented by two ligand-centered non-bonding orbitals e_g (Fig. 19). Filling up this level makes it possible to increase the maximum number of electrons on the bonds of the cluster core up to 18. This effect explains the existence of clusters with the same charge but with different numbers of valence electrons of the interstitial atom and the number of CSEs, e.g. Zr_6CCl_{14} (14 CSEs) [96] and Zr_6FeI_{14} (18 CSEs) [114]. The non-bonding nature of orbitals e_g explains low oxidation potentials of zirconium clusters with interstitial *d*-block atoms to cause instability in some discrete clusters of this type in solutions [115].

Interstitial atom in the trigonal-prismatic environment. These fragments are formally composed of two triangles $\{M_3\}$ and three *M–M* bonds between them. Whereas the octahedral clusters are characterized by 12 covalent bonds whose lengths usually differ only slightly, the prismatic clusters have 9 *M–M* bonds and the bond lengths inside the triangular fragments usually differ significantly from the bond lengths between the atoms of the neighboring triangles. We now consider the electronic structure of such clusters using anion $[Nb_6SBr_{18}]^{4-}$ as an example [116]. In this cluster, 14 CSEs are localized on 7 metal-centered bonding orbitals with symmetries a_1', a_2'', e', and e''. In contrast to the above octahedral zirconium clusters, the valence AOs of the interstitial atom have a small contribution to these MOs, so that the sulfur atom can be considered an electron acceptor (anion S^{2-}). The average length of six Nb–Nb bonds constituting the edges of the prism's triangular faces is 2.97 Å to signify covalent bonding. At the same time, the Nb–Nb distance between the triangular faces is as long as 3.28 Å. The quantum chemical calculations showed that the interactions of Nb atoms between the triangular faces have a weakly bonding nature mostly determined by the Nb–μ_6-S bonds with a length of 2.37 Å.

A series of trigonal-prismatic clusters $[W_6ZCl_{18}]^{n-}$ demonstrates the impact of the number of CSEs on the geometry and electronic structure of similar clusters [98]. The average W–W distance in the neutral cluster $[W_6CCl_{18}]$ is 2.743 Å in triangular fragments and 2.930 Å between them [51]. In this cluster, 14 CSEs are located on 7 bonding orbitals similarly to the niobium cluster discussed above, and the carbon atom is considered to be an electron acceptor with the formal oxidation state 4–. One-electron reduction yields anion $[W_6CCl_{18}]^-$ which is formed in the salts $A[W_6CCl_{18}]$ and has 15 CSEs. The average W–W distances in this anion are 2.74 Å and 2.93 Å in triangular fragments and between them, respectively. Finally, the "substitution" of carbon atom by a nitrogen atom yields an 16-electron anion $[W_6NCl_{18}]^-$ with the corresponding W–W distances equal to 2.6518 Å and 3.0705 Å [55]. A similar geometry is demonstrated by the 16-electron anion $[W_6CCl_{18}]^{2-}$ [100]. Thus, the *M–M* interaction between atoms W of triangular prism faces tends to increase as the number of CSEs increases from 14 to 16; at the same time, the interaction between the triangular faces decreases. This is due to the localization of additional electrons on the orbital $2a_2''$, which is antibonding with respect to the atoms of the neighboring triangles (Fig. 20).

As anion $[W_6NCl_{18}]^-$ is reduced still further, orbital e' is filled and becomes bonding with respect to one of W–W bonds between the triangular fragments while the cluster symmetry is distorted, which is especially evident on the example of anion $[W_6NCl_{18}]^{3-}$ (18 CSEs) [55]. One of the W–W bonds between the triangular fragments is shortened significantly whereas the bonds in the triangular plane are elongated. A similar effect is caused by the reduction of anion $[W_6CCl_{18}]^{2-}$ [100].

Another large group of clusters containing an interstitial atom in a trigonal prismatic environment is formed by twelve-nuclear rhenium clusters. These clusters exist in the form of stable anions with 46 or 48 CSEs. The 46-electron clusters based on the $\{Re_{10}^{III}Re_2^{IV}\}$ metal center can be formally considered as a combination two 23-electron octahedral

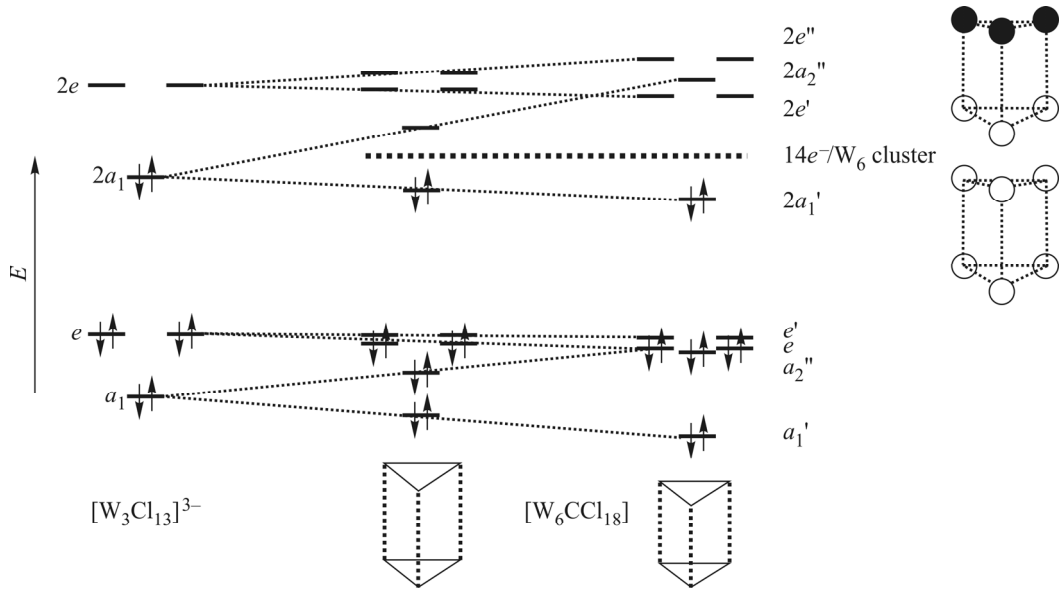

Fig. 20. Changes in the system of molecular orbitals of tungsten complexes [100].

cores{Re_6S_7C}. These clusters are diamagnetic, i.e. their molecular orbitals are delocalized over all atoms of the cluster core. Indeed, the DFT calculation of the electronic structure of the 46-electron anion $[Re_{12}CS_{14}(\mu\text{-}S)_3(CN)_6]^{6-}$ showed that HOMO and LUMO anions are mainly localized on the atoms of the prismatic fragment {$Re_3(\mu_6\text{-}C)(\mu\text{-}S)_3Re_3$} [61]. The contribution of 3*p* orbitals of the atoms of μ-S ligands to the HOMO of {$Re_3(\mu_6\text{-}C)(\mu\text{-}S)_3Re_3$} exceeds 80%. In the $[Re_{12}CS_{14}(\mu\text{-}S)_3(CN)_6]^{6-}$ anion , the contribution of Re *d* orbitals and $2p_z$ orbitals of the μ_6-C ligand is higher in LUMO orbitals than in HOMO orbitals. Short Re–Re contacts between the atoms of the triangular prism faces, as well as Re–C bonds, are bonding in nature, while long Re–Re contacts between the octahedra are antibonding in nature. Thus, similarly to the case of prismatic tungsten clusters, the main contribution to the bonding of triangular fragments is due to the bonds between the metal atoms and the bridging ligands.

The geometry and the electron density distribution of the 48-electron anion $[Re_{12}CS_{14}(\mu\text{-}S)_3(CN)_6]^{8-}$ differ significantly from those of its 46-electron analog. Thus, the distance between rhenium atoms of the neighboring octahedral fragments is 3.168 Å in the 48-electron cluster anion and 2.901 Å in the 46-electron cluster. Also, the 48-electron cluster exhibits a larger distortion of {Re_6} octahedra, which is manifested in increased differences between the lengths of Re–Re bonds between rhenium atoms located on the outer and inner faces of the octahedra. These processes correspond to the filling of the 31*a*″ orbital localized on the atoms of the prismatic fragment and its significant energy decrease [61]. The further analysis of the electronic structure showed that the charge of such cluster anions can be controlled by an external electromagnetic field, which can be possibly used in the design of molecular switchers based on the {Re_{12}} clusters [117].

Modifying bridging ligands significantly affects spectroscopic characteristics of bioctahedral clusters. Thus, when $\mu\text{-}S^{2-}$ ligands were oxidized to $(\mu\text{-}SO_2)^{2-}$ ligands while preserving the number of their CSEs, the solution's color changed abruptly from brown to purple and then to green. The corresponding change in the electronic absorption spectrum was characterized by the appearance of broad absorption bands at 529 nm and 593 nm, respectively, whereas the absorption spectrum of the cluster anion $[Re_{12}CS_{14}(\mu\text{-}S)_3(CN)_6]^{6-}$ is characterized by the bands at 440 nm and 510 nm. A TD–DFT analysis of electronic spectra showed that transitions in the visible region for the $[Re_{12}CS_{14}(\mu\text{-}S)_3(CN)_6]^{6-}$ cluster correspond to electron transfer from the *p* orbitals of $\mu\text{-}S^{2-}$ ligands to the valence *d* orbitals of Re atoms (ligand-to-metal charge transfer, LMCT). At the same time, the orbitals responsible for the charge transfer of anions $[Re_{12}CS_{14}(\mu\text{-}SO_2)_3(CN)_6]^{6-}$ and $[Re_{12}CS_{14}(\mu\text{-}SO_2)_2(\mu\text{-}SO_3)(CN)_6]^{6-}$ are mainly composed of rhenium orbitals, so that these transitions can be considered as

a metal-to-metal charge transfer (MMCT). All orbitals participating in the above processes are largely localized on the atoms of the central prismatic fragment $\{Re_3(\mu_6\text{-}C)(\mu\text{-}L)_3Re_3\}$ [68].

The most significant changes in the spectroscopic properties of twelve-nuclear rhenium clusters were observed upon substituting the ligands in the prismatic fragment by the halide-anions Cl^- or Br^- while the clusters were simultaneously reduced to 48-electron anions $[Re_{12}CS_{14}(\mu\text{-}Cl)_3Cl_6]^{5-}$, $[Re_{12}CS_{14}(\mu\text{-}Br)_3Cl_6]^{5-}$ and $[Re_{12}CS_{14}(\mu\text{-}Br)_3Br_6]^{5-}$ [72]. In this case, the HOMO–LUMO increases significantly up to ~3.5 eV. Also, the LUMO structure exhibits a substantial contribution of μ_3 ligands to cause effective charge transfer from the metal atoms to the ligands. In turn, this causes photoluminescence whose parameters are similar to those observed in the luminescence of octahedral rhenium clusters.

CONCLUSIONS

As can be seen from the presented material, the chemistry of cluster complexes with interstitial atoms of group 3-7 metals is quite diverse. In the most of discussed examples, the interstitial atom plays the key role in the formation and stability of the cluster core by donating its electrons to the molecular orbitals of the metal cluster. The key role of interstitial atoms is testified by the calculations of the electronic structure of such complexes. Many specific properties of cluster compounds are determined by the cluster core, and the interstitial atoms significantly change the properties of such compounds: the composition of the formed phases, their geometry and electronic properties. As it was mentioned in the review, the interstitial atom enters into the metal cluster at the stage when the cluster compounds is being formed, and it cannot be removed without destroying the cluster. On the other hand, the examples of compounds that are fairly stable upon the dissolution of the cluster fragment (first of all, $[Re_{12}CS_{17}(CN)_6]^{8-/6-}$, $[W_6(C/N)Cl_{18}]^{n-}$, and $[Zr_6ZX_{18}]^{n-}$) allow using these cluster complexes in redox processes and reactions of ligand substitution with the goal of “fine tuning” of their physical properties. Despite quite a long history of this field of chemistry, its further progress seems to be possible as far as the preparation and application of transition metal cluster compounds containing interstitial heteroatoms.

FUNDING

The reported study was funded by RFBR, project number 19-13-50318.

CONFLICT OF INTERESTS

The authors declare that they have no conflict of interests.

REFERENCES

1. F. A. Cotton. *Quart. Rev*., *Chem. Soc*., **1966**, *20*, 389.
2. J. C. P. Gabriel, K. Boubekeur, S. Uriel, and P. Batail. *Chem. Rev*., **2001**, *101*, 2037.
3. T. G. Gray. *Coord. Chem. Rev*., **2003**, *243*, 213.
4. V. Y. Fedorov, Y. V. Mironov, N. G. Naumov, M. N. Sokolov, and V. P. Fedin. *Usp. Khim*., **2007**, *76*, 571.
5. M. N. Sokolov, N. G. Naumov, P. P. Samoylov, and V. P. Fedin. Clusters and Cluster Assemblies. In: Comprehensive Inorganic Chemistry II, Vol. 2 / Eds. J. Reedijk and K. Poeppelmeier. Elsevier: Oxford, **2013**, 271.
6. G. Meyer. Rare Earth Metal Cluster Complexes. In: The Rare Earth Elements: Fundamentals and Applications / Ed. D. A. Atwood. Wiley, **2012**, 415.
7. P. Lemoine, J. F. Halet, and S. Cordier. *Struct. Bonding*, **2019**, *180*, 143.
8. M. Ströbele and H. J. Meyer. *Dalton Trans*., **2019**, *48*, 1547.
9. M. A. Mikhaylov and M. N. Sokolov. *Eur. J. Inorg. Chem*., **2019**, *2019*, 4181.
10. H. Schäfer and H. G. Schnering. *Angew. Chem*., **1964**, *76*, 833.

11. A. Simon. *Angew. Chem*., *Int. Ed*., **1981**, *20*, 1.
12. A. Simon, F. Böttcher, and J. K. Cockcroft. *Angew. Chem*., *Int. Ed*., **1991**, *30*, 101.
13. F. Böttcher, A. Simon, R.K. Kremer, H. Buchkremer-Hermanns, and J. K. Cockcroft. *Z. Anorg. Allg. Chem*., **1991**, *598*, 25.
14. D. J. Hinz and G. Meyer. *J. Chem. Soc*., *Chem.Commun*., **1994**, 125.
15. F. A. Cotton, J. Lu, M. Y. Shang, and W. A. Wojtczak. *J. Am. Chem. Soc*., **1994**, *116*, 4364.
16. L. F. Chen and F. A. Cotton. *J. Clust. Sci*., **1998**, *9*, 63.
17. L. F. Chen, F. A. Cotton, and W. A. Wojtczak. *Inorg. Chem*., **1997**, *36*, 4047.
18. L. F. Chen, F. A. Cotton, W. T. Klooster, and T. F. Koetzle. *J. Am. Chem. Soc*., **1997**, *119*, 12175.
19. L. F. Chen and F. A. Cotton. *Inorg. Chim. Acta*, **1997**, *257*, 105.
20. F. A. Cotton, L. F. Chen and A. J. Schultz. *C. R. Acad. Sci*., *Ser. IIb*, **1996**, *323*, 539.
21. L. F. Chen, F. A. Cotton, and W. A. Wojtczak. *Inorg. Chem*., **1996**, *35*, 2988.
22. L. F. Chen, F. A. Cotton, and W. A. Wojtczak. *Inorg. Chim. Acta*, **1996**, *252*, 239.
23. L. F. Chen, F. A. Cotton, and W. A. Wojtczak. *Angew. Chem*., *Int. Ed*., **1995**, *34*, 1877.
24. J. Zhang, R. P. Ziebarth, and J. D. Corbett. *Inorg. Chem*., **1992**, *31*, 614.
25. F. A. Cotton, X. J. Feng, M. Y. Shang, and W. A. Wojtczak. *Angew. Chem*., *Int. Ed*., **1992**, *31*, 1050.
26. F. Rogel and J. D. Corbett. *J. Am. Chem. Soc*., **1990**, *112*, 8198.
27. X. B. Xie and T. Hughbanks. *Inorg. Chem*., **2002**, *41*, 1824.
28. A. Bernsdorf and M. Köckerling. *Eur. J. Inorg. Chem*., **2011**, 4057.
29. H. W. Rohm and M. Köckerling. *Inorg. Chem*., **2008**, *47*, 2234.
30. X. B. Xie, J. H. Reibenspies, and T. Hughbanks. *J. Am. Chem. Soc*., **1998**, *120*, 11391.
31. X. Xie and T. Hughbanks. *Solid State Sci*., **1999**, *1*, 463.
32. X. B. Xie and T. Hughbanks. *Angew. Chem*., *Int. Ed*., **1999**, *38*, 1777.
33. X. B. Xie and T. Hughbanks. *Inorg. Chem*., **2000**, *39*, 555.
34. X. B. Xie, J. N. Jones, and T. Hughbanks. *Inorg. Chem*., **2001**, *40*, 522.
35. J. S. Wilkes, J. A. Levisky, R. A. Wilson, and C. L. Hussey. *Inorg. Chem*., **1982**, *21*, 1263.
36. A. A. Fannin, D. A. Floreani, L. A. King, J. S. Landers, B. J. Piersma, D. J. Stech, R. L. Vaughn, J. S. Wilkes, and J. L. Williams. *J. Phys. Chem*., **1984**, *88*, 2614.
37. D. Sun and T. Hughbanks. *Inorg. Chem*., **2000**, *39*, 1964.
38. Y. C. Tian and T. Hughbanks. *Inorg. Chem*., **1995**, *34*, 6250.
39. R. Y. Qi and J. D. Corbett. *Inorg. Chem*., **1994**, *33*, 5727.
40. E. J. Wu, M. A. Pell, and H. S. Genin, J.A. Ibers. *J. Alloys Compd*., **1998**, *278*, 123.
41. H. Womelsdorf and H. J. Meyer. *Angew. Chem*., *Int. Ed*., **1994**, *33*, 1943.
42. A. N. Fitch, S. A. Barrett, B. E. F. Fender, and A. Simon. *J. Chem. Soc*., *Dalton. Trans*., **1984**, 501.
43. A. Simon, F. Stollmaier, D. Gregson, and H. Fuess. *J. Chem. Soc*., *Dalton. Trans*., **1987**, 431.
44. H. Imoto and J. D. Corbett. *Inorg. Chem*., **1980**, *19*, 1241.
45. H. J. Meyer and J. D. Corbett. *Inorg. Chem*., **1992**, *31*, 4276.
46. H. J. Meyer and J. D. Corbett. *Inorg. Chem*., **1991**, *30*, 963.
47. D. Fenske, A. Grissinger, M. Loos, and J. Magull. *Z. Anorg. Allg. Chem*., **1991**, *598*, 121.
48. J. L. Krinsky, L. L. Anderson, J. Arnold, and R. G. Bergman. *Inorg. Chem*., **2008**, *47*, 1053.
49. D. Salloum, R. Gautier, M. Potel, and P. Gougeon. *Angew. Chem*., *Int. Ed*., **2005**, *44*, 1363.
50. C. Perrin and M. Sergent. *J. Chem. Res*., *Synop*., **1983**, 38.
51. Y. Q. Zheng, H. G. von Schnering, J. H. Chang, Y. Grin, G. Engelhardt, and G. Heckmann. *Z. Anorg. Allg. Chem*., **2003**, *629*, 1256.
52. E. J. Welch, N. R. M. Crawford, R. G. Bergman, and J. R. Long. *J. Am. Chem. Soc*., **2003**, *125*, 11464.
53. M. Strobele and H. J. Meyer. *Inorg. Chem*., **2010**, *49*, 5986.

54. A. Mos, M. Ströbele, and H. J. Meyer. *Z. Anorg. Allg. Chem*., **2015**, *641*, 2245.
55. E. J. Welch, C. L. Yu, N. R. M. Crawford, and J. R. Long. *Angew. Chem*., *Int. Ed*., **2005**, *44*, 2549.
56. M. Weisser, R. Burgert, H. Schnöckel, and H. J. Meyer. *Z. Anorg. Allg. Chem*., **2008**, *634*, 633.
57. M. Weisser, M. Ströbele, and H. J. Meyer. *C. R. Chim*., **2005**, *8*, 1820.
58. P. A. Abramov, A. V. Rogachev, M. A. Mikhailov, A. V. Virovets, E. V. Peresypkina, M. N. Sokolov, and V. P. Fedin. *Russ. J. Coord. Chem*., **2014**, *40*, 259.
59. E. J. Welch and J. R. Long. *Angew. Chem*., *Int. Ed*., **2007**, *46*, 3494.
60. A. R. Fout, Q. L. Zhao, D. N. J. Xiao, and T. A. Betley. *J. Am. Chem. Soc*., **2011**, *133*, 16750.
61. Y. V. Mironov, N. G. Naumov, S. G. Kozlova, S. J. Kim, and V. E. Fedorov. *Angew. Chem*., *Int. Ed*., **2005**, *44*, 6867.
62. V. E. Fedorov, N. G. Naumov, Y. V. Mironov, S. G. Kozlova, and S. P. Gabuda. *J. Struct. Chem*., **2011**, *52*(5), 1000.
63. Y. V. Mironov, S. G. Kozlova, S. J. Kim, W. S. Sheldrick, and V. E. Fedorov. *Polyhedron*, **2010**, *29*, 3283.
64. Y. M. Gayfulin, M. R. Ryzhikov, D. G. Samsonenko, and Y. V. Mironov. *Polyhedron*, **2018**, *151*, 426.
65. V. E. Fedorov, S. P. Gabuda, S. G. Kozlova, Y. M. Gayfulin, Y. V. Mironov, M. R. Rizhikov, and N. F. Uvarov. *Croat. Chem. Acta*, **2012**, *85*, 113.
66. R. Chevrel, M. Sergent, and J. Prigent. *Mater. Res. Bull*., **1974**, *9*, 1487.
67. Y. M. Gayfulin, A. I. Smolentsev, S. G. Kozlova, V. V. Yanshole, and Y. V. Mironov. *Polyhedron*, **2014**, *68*, 334.
68. Y. V. Mironov, Y. M. Gayfulin, S. G. Kozlova, A. I. Smolentsev, M. S. Tarasenko, A. S. Nizovtsev, and V. E. Fedorov. *Inorg. Chem*., **2012**, *51*, 4359.
69. Y. M. Gayfulin, A. I. Smolentsev, L. V. Yanshole, S. G. Kozlova, and Y. V. Mironov. *Eur. J. Inorg. Chem*., **2016**, 4066.
70. T. I. Lappi, Y. M. Gayfulin, A. I. Smolentsev, and Y. V. Mironov. *J. Struct. Chem*., **2017**, *58*(4), 835.
71. Y. M. Gayfulin, A. I. Smolentsev, S. G. Kozlova, I. N. Novozhilov, P. E. Plyusnin, N. B. Kompankov, and Y. V. Mironov. *Inorg. Chem*., **2017**, *56*, 12389.
72. Y. M. Gayfulin, K. A. Brylev, M. R. Ryzhikov, D. G. Samsonenko, N. Kitamura, and Y. V. Mironov. *Dalton Trans*., **2019**, *48*, 12522.
73. N. G. Naumov, A. V. Virovets, and V. E. Fedorov. *J. Struct. Chem*., **2000**, *41*(3), 499.
74. V. E. Fedorov, N. G. Naumov, Y. V. Mironov, A. V. Virovets, S. B. Artemkina, K. A. Brylev, S. S. Yarovoi, O. A. Efremova, and U. H. Paek. *J. Struct. Chem*., **2002**, *43*(4), 669.
75. E. V. Alexandrov, A. V. Virovets, V. A. Blatov, and E. V. Peresypkina. *Chem. Rev*., **2015**, *115*, 12286.
76. Y. V. Mironov, N. G. Naumov, S. J. Kim, and V. E. Fedorov. *Russ. J. Coord. Chem*., **2007**, *33*, 279.
77. Y. M. Gayfulin, A. I. Smolentsev, and Y. V. Mironov. *J Coord. Chem*., **2011**, *64*, 3832.
78. V. P. Fedin, I. V. Kalinina, A. V. Virovets, N. V. Podberezskaya, I. S. Neretin, and Y. L. Slovokhotov. *Chem. Commun*., **1998**, 2579.
79. V. P. Fedin, I. V. Kalinina, A. V. Virovets, and D. Fenske. *Russ. Chem. Bull*., **2001**, *50*, 930.
80. T. Schleid and G. Meyer. *J. Less-Common Met*., **1987**, *127*, 161.
81. N. Gerlitzki, S. Hammerich, I. Pantenburg, and G. Meyer. *Z. Anorg. Allg. Chem*., **2006**, *632*, 2024.
82. G. Meyer and S. Uhrlandt. *Angew. Chem*., *Int. Ed*., **1993**, *32*, 1318.
83. S. Uhrlandt and G. Meyer. *Z. Anorg. Allg. Chem*., **1994**, *620*, 1872.
84. S. Uhrlandt and T. Heuer, G. Meyer. *Z. Anorg. Allg. Chem*., **1995**, *621*, 1299.
85. S. Uhrlandt and G. Meyer. *Z. Anorg. Allg. Chem*., **1995**, *621*, 1466.
86. H. M. Artelt, T. Schleid, and G. Meyer. *Z. Anorg. Allg. Chem*., **1992**, *618*, 18.
87. T. Hughbanks and J. D. Corbett. *Inorg. Chem*., **1989**, *28*, 631.
88. T. Hughbanks and J. D. Corbett. *Inorg. Chem*., **1988**, *27*, 2022.
89. H. Mattausch, C. Hoch, and A. Simon. *Z. Anorg. Allg. Chem*., **2005**, *631*, 1423.
90. J. D. Corbett. *Inorg. Chem*., **2000**, *39*, 5178.
91. J. D. Corbett. *J. Chem. Soc*., *Dalton. Trans*., **1996**, 575.

92. J. D. Corbett. *J. Alloys Compd*., **1995**, *229*, 10.
93. R. P. Ziebarth and J. D. Corbett. *Acc. Chem. Res*., **1989**, *22*, 256.
94. J. Zhang and J. D. Corbett. *J. Less-Common Met*., **1989**, *156*, 49.
95. R. P. Ziebarth and J. D. Corbett. *Inorg. Chem*., **1989**, *28*, 626.
96. R. P. Ziebarth and J. D. Corbett. *J. Am. Chem. Soc*., **1985**, *107*, 4571.
97. J. D. Smith and J. D. Corbett. *J. Am. Chem. Soc*., **1985**, *107*, 5704.
98. M. Weisser, S. Tragl, and H. J. Meyer. *J. Clust. Sci*., **2009**, *20*, 249.
99. M. Weisser, R. Burgert, H. Schnöckel, and H. J. Meyer. *Z. Anorg. Allg. Chem*., **2008**, *634*, 633.
100. E. J. Welch, N. R. M. Crawford, R. G. Bergman, and J. R. Long. *J. Am. Chem. Soc*., **2003**, *125*, 11464.
101. N. G. Naumov, A. V. Virovets, M. N. Sokolov, S. B. Artemkina, and V. E. Fedorov. *Angew. Chem*., *Int. Ed*., **1998**, *37*, 1943.
102. S. S. Yarovoi, Y. V. Mironov, D. Y. Naumov, Y. V. Gatilov, S. G. Kozova, S. J. Kim, and V. E. Fedorov. *Eur. J. Inorg. Chem*., **2005**, 3945.
103. A. Simon, E. Warkentin, and R. Masse. *Angew. Chem*., *Int. Ed*., **1981**, *20*, 1013.
104. M. Bruhmann and G. Meyer. *Eur. J. Inorg. Chem*., **2010**, 2609.
105. H. Mattausch, G. V. Vajenine, O. Oeckler, R. K. Kremer, and A. Simon. *Z. Anorg. Allg. Chem*., **2001**, *627*, 2542.
106. M. W. Payne, M. Ebihara, and J. D. Corbett. *Angew. Chem*., *Int. Ed*., **1991**, *30*, 856.
107. S. M. Kauzlarich, T. Hughbanks, J. D. Corbett, P. Klavins, and R. N. Shelton. *Inorg. Chem*., **1988**, *27*, 1791.
108. H. Mattausch, R. K. Kremer, A. Simon, and W. Bauhofer. *Z. Anorg. Allg. Chem*., **1993**, *619*, 741.
109. C. Bauhofer, H. Mattausch, G. J. Miller, W. Bauhofer, R. K. Kremer, and A. Simon. *J. Less-Common Met*., **1990**, *167*, 65.
110. H. Mattausch, O. Oeckler, and A. Simon. *Z. Anorg. Allg. Chem*., **2008**, *634*, 503.
111. H. Mattausch, M. C. Schaloske, C. Hoch, and A. Simon. *Z. Anorg. Allg. Chem*., **2008**, *634*, 498.
112. H. Mattausch, M. C. Schaloske, C. Hoch, C. Zheng, and A. Simon. *Z. Anorg. Allg. Chem*., **2008**, *634*, 491.
113. R. P. Ziebarth and J. D. Corbett. *J. Am. Chem. Soc*., **1989**, *111*, 3272.
114. T. Hughbanks, G. Rosenthal, and J. D. Corbett. *J. Am. Chem. Soc*., **1986**, *108*, 8289.
115. X. Xie and T. Hughbanks. *Inorg. Chem*., **2000**, *39*, 555.
116. H. Womelsdorf and H. J. Meyer. *Angew. Chem*., *Int. Ed*., **1994**, *33*, 1943.
117. S. P. Gabuda, S. G. Kozlova, Y. V. Mironov, and V. E. Fedorov. *Nanoscale Res. Lett*., **2009**, *4*, 1110.